

Fall 2010

A rotating ring-disk study of interactions among SPS, cuprous ions, and oxygen

Yi-Hsin Chen

University of New Hampshire, Durham

Follow this and additional works at: <https://scholars.unh.edu/dissertation>

Recommended Citation

Chen, Yi-Hsin, "A rotating ring-disk study of interactions among SPS, cuprous ions, and oxygen" (2010). *Doctoral Dissertations*. 533.
<https://scholars.unh.edu/dissertation/533>

This Dissertation is brought to you for free and open access by the Student Scholarship at University of New Hampshire Scholars' Repository. It has been accepted for inclusion in Doctoral Dissertations by an authorized administrator of University of New Hampshire Scholars' Repository. For more information, please contact nicole.hentz@unh.edu.

**A ROTATING RING-DISK STUDY OF INTERACTIONS AMONG SPS,
CUPROUS IONS, AND OXYGEN**

BY

YI-HSIN CHEN

M. S., National Cheng Kung University, 2002

B. S., Chang Gung University, 2000

DISSERTATION

Submitted to the University of New Hampshire

in Partial Fulfillment of

the Requirements for the Degree of

Doctor of Philosophy

in

Chemical Engineering

September 2010

UMI Number: 3430787

All rights reserved

INFORMATION TO ALL USERS

The quality of this reproduction is dependent upon the quality of the copy submitted.

In the unlikely event that the author did not send a complete manuscript and there are missing pages, these will be noted. Also, if material had to be removed, a note will indicate the deletion.



UMI 3430787

Copyright 2010 by ProQuest LLC.

All rights reserved. This edition of the work is protected against unauthorized copying under Title 17, United States Code.



ProQuest LLC
789 East Eisenhower Parkway
P.O. Box 1346
Ann Arbor, MI 48106-1346

This dissertation has been examined and approved.



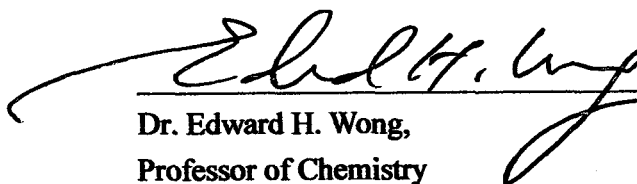
Dissertation Director, Dr. Dale P. Barkey,
Professor of Chemical Engineering



Dr. Russell Carr,
Professor of Chemical Engineering



Dr. Xiaowei Teng,
Assistant Professor of Chemical Engineering



Dr. Edward H. Wong,
Professor of Chemistry



Dr. James Krzanowski,
Professor of Mechanical Engineering

July 29, 2010

Date

ACKNOWLEDGEMENTS

I would like to thank my advisor, Dr. Dale P. Barkey, for his patient guidance, knowledge sharing, and invaluable advice on my research during these years. Without his guidance and encouragement, I could not have finished this dissertation. I deeply appreciate all the opportunities he gave me about the industrial connections and electrochemical expertise under his direction.

I would like to thank Dr. Russell Carr, Dr. Xiaowei Teng, Dr. Edward H. Wong, and Dr. James Krzanowski for being the committee members and giving the insightful comments to complete my research.

I am grateful to Mr. John E. Newell for his assistance of laboratory troubleshooting and experimental setup and I also appreciate Mrs. Nancy Brady Littlefield for her help during my study at UNH.

I am thankful to Sheik Ansar, Ashleigh Kreider, and Joseph Iulucci for their help in course study, lab research, and miscellaneous US living problems.

I would like to thank Dr. Zhenqiu Liu, the director of NEXX Systems, for giving me the opportunity of summer internship to extend my research and recover all the industrial information that I missed during the study at the university. More importantly, without his encouragement and recommendation, I may not have the chance to carry out my goal to study in US.

Last, but not least, I want to thank my parents and my wife Wei-Hsuan Chung. Especially my wife, she is always with me to share my frustrations and support me with all she can do.

TABLE OF CONTENTS

ACKNOWLEDGEMENTS	iii
LIST OF TABLES	vi
LIST OF FIGURES	vii
ABSTRACT.....	x
CHAPTER I: INTRODUCTION.....	1
1.1 Objectives	1
1.2 Electrodeposition	2
1.3 Additives and current wave train in copper electrodeposition.....	3
1.4 Rotating disk electrode and rotating ring-disk electrode	6
CHAPTER II: LITERATURE REVIEW	8
2.1 Copper electrodeposition and plating bath	8
2.2 Effect of chloride	8
2.3 Effect of polyethylene glycol.....	9
2.4 Effect of bis-(3-sulfopropyl)-disulfide.....	14
2.5 Mechanisms of via filling	19
2.6 Via filling with oxygen purging	22
CHAPTER III: EXPERIMENTAL	24
3.1 Introduction.....	24
3.1.1 Reaction diffusion model.....	24
3.2 Experimental setup and instrumentation.....	28
3.2.1 Electroplating cell	28
3.2.2 Bipotentiostat and modulated speed rotator.....	29
3.2.3 Chemical reagents.....	30
3.2.4 Experimental matrix.....	30
CHAPTER IV: RESULTS AND DISCUSSION	32
4.1 Effect of SPS concentration	32

4.1.1 Ring current transients under air.....	33
4.1.2 Ring current transients under oxygen and argon	39
4.1.3 Cu (I) generation at the disk under air, oxygen, and argon	41
4.2 Effect of rotation speed	46
4.2.1 Ring current transients under air – with and without additives	46
4.2.2 Ring current transients under oxygen and argon	47
4.2.3 Cu (I) generation at the disk under air, oxygen, and argon.....	54
4.3 Effect of disk stripping potential.....	59
4.3.1 Ring current transients with air saturated – with and without additives.....	59
4.3.2 Ring current transients under oxygen and argon	60
4.3.3 Cu (I) generation at the disk under air, oxygen, and argon.....	65
CHAPTER V: CONCLUSIONS AND RECOMMENDATIONS FOR FUTURE WORK	70
5.1 Conclusions.....	70
5.2 Recommendations for future work	71
LITERATURE CITED.....	73

LIST OF TABLES

Table 3.1 Copper electroplating solution components.....	30
Table 3.2 Experimental matrix.....	31
Table 4.1 Bipotentiostat parameters of a1, a2, b1, and b2 procedures	32
Table 4.2 Ratio of Cu (I) partial current to total disk current at successive runs under various SPS concentrations.....	42
Table 4.3 Average Cu (I) partial current from disk and ring charge with Cu (I) generation (procedure a2) under various SPS concentrations	44
Table 4.4 Ratio of Cu (I) partial current to total disk current at successive runs under rotation speed variation.....	55
Table 4.5 Average Cu (I) partial current ratio from disk and ring charge with Cu (I) generation (procedure a2)	57
Table 4.6 Ratio of Cu (I) partial current to total disk current at successive runs under stripping potential variation	66
Table 4.7 Average Cu (I) partial current ratio from disk and ring charge with Cu (I) generation (procedure a2)	68

LIST OF FIGURES

Figure 1.1 Types of profile evolution in via plating	5
Figure 1.2 Structure of (a) rotating disk electrode and (b) rotating ring-disk electrode	7
Figure 2.1 Effect of PEG and Cl^- on the polarization behavior through RDE at 900 rpm..	12
Figure 2.2 Adsorption of spherical PEG molecules on copper	12
Figure 2.3 Illustration of synergetic adsorption of PEG and Cl^-	13
Figure 2.4 Filling performance as a function of PEG molecule weight	13
Figure 2.5 Chemical structures of (a) SPS, and (b) MPS	14
Figure 2.6 Hysteretic η -i curves with various SPS concentrations in the presence of PEG and Cl^- additives.....	17
Figure 2.7 Behavior of MPS, PDT, and PDSA at 1 ppm when added to the basic electrolyte	18
Figure 2.8 Potentiostatic behavior of PEG-SPS- Cl^- and PEG-MPS- Cl^- systems	18
Figure 2.9 Model for transient additive interactions during the bottom-up fill of high aspect ratio vias.....	21
Figure 2.10 Schematic of via filling with dissolved oxygen	22
Figure 2.11 Micrographs of via cross section in two-stage plating process without and with O_2 purging	23
Figure 3.1 Bottom-up filling with O_2 purging and simulated interactions at a RRDE with deposition on the ring and concurrent stripping on the disk.....	25
Figure 3.2 Cu deposition on the ring without and with Cu (I) generation on the disk	26
Figure 3.3 Cu deposition and stripping in procedure b1 and b2.....	27
Figure 3.4 Electroplating cell and electrode	28
Figure 3.5 Bipotentiostat and modulated speed rotator	29
Figure 4.1 Ring current transients under air without SPS	35
Figure 4.2 Ring current transients under air with SPS.....	36
Figure 4.3 Ring current transients of 10 th run without and with Cu (I) generation at the disk under air	37
Figure 4.4 Successive ring integrated currents without and with Cu (I) production at the	

disk. Experiments are performed under air.....	38
Figure 4.5 Successive ring integrated currents without and with Cu (I) production at the disk.....	40
Figure 4.6 Cu(I) partial current at disk as a function of SPS concentration under different gases.....	43
Figure 4.7 (a) Average ring charge with Cu (I) generation, and (b) Increased percentage of ring charge from a1 to a2 as a function of Cu (I) partial current at disk by SPS concentration variation under air, oxygen, and argon.....	45
Figure 4.8 Ring current transients under air without and with Cu (I) generation at the disk at 5 rpm	48
Figure 4.9 Ring current transients under air without and with Cu (I) generation at the disk at 400 rpm	49
Figure 4.10 Ring current transients of 10 th run without and with Cu (I) generation at the disk versus rotation speed.....	50
Figure 4.11 Successive ring integrated current without and with Cu (I) production at the disk.....	51
Figure 4.12 The rotation speed effect of steady ring current density difference of the 10 th run from a1 to a2.....	52
Figure 4.13 Successive ring integrated current without and with Cu (I) production at the disk.....	53
Figure 4.14 Average Cu (I) partial current at the disk as a function of rotation speed under various gases	56
Figure 4.15 Average ring charge with Cu (I) generation and increased percentage of ring charge from a1 to a2 as a function of Cu (I) partial current at disk by rotation speed variation under air, oxygen, and argon.....	58
Figure 4.16 Ring current transients under air without and with Cu (I) generation at the disk at 100 mV.....	61
Figure 4.17 Ring current transients of 10 th run without and with Cu (I) generation at the disk under air.....	62
Figure 4.18 Successive ring integrated current without and with Cu (I) production at the disk.....	63

Figure 4.19 Successive ring integrated current without and with Cu (I) production at the disk..... 64

Figure 4.20 Cu (I) partial current at the disk as a function of stripping potential with various gases..... 67

Figure 4.21 Average ring charge with Cu (I) generation and increased percentage of ring charge from a1 to a2 as a function of Cu (I) partial current at disk by strip potential variation under air, oxygen, and argon..... 69

ABSTRACT

A ROTATING RING-DISK STUDY OF INTERACTIONS AMONG SPS, CUPROUS IONS, AND OXYGEN

by

Yi-Hsin Chen

University of New Hampshire, September, 2010

The most common additives in copper plating baths for deep via filling are chloride, polyethylene glycol (PEG), a suppressor, and bis-(3-sulfopropyl)-disulfide (SPS), an accelerant. The copper in acid plating baths is provided by a Cu (II) salt. Cu (I) may be present as well and it influenced the effectiveness of SPS. In this investigation, the interactions among SPS, Cu (I) and oxygen were studied by rotating ring-disk voltammetry. The ring electrode acted as a plating substrate, while Cu (I) was generated at the disk by anodic dissolution of copper. Because Cu (I) is consumed by reaction with oxygen, the experiments were carried out under air, oxygen, or argon atmospheres.

When SPS is present in the solution, a sudden kinetic acceleration is observed at the ring during Cu (I) generation at the disk. By comparing the ring deposition rate without and with Cu (I) generation at the disk, it is found that deposition is accelerated by higher levels of Cu (I) and SPS. The result is considered in light of the hypothesis that the true accelerant is formed by homogeneous reaction of SPS and Cu (I).

CHAPTER I: INTRODUCTION

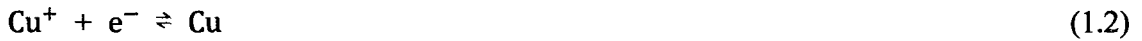
1.1 Objectives

The most common additives of copper plating bath for deep via filling are chloride, polyethylene glycol (PEG) and bis-(3-sulfopropyl)-disulfide (SPS). In the PEG-SPS-Cl⁻ additive system, PEG acts as a suppressor. SPS is added as an accelerant to disrupt the PEG-Cl⁻ blocking layer, and it selectively increases the deposition rate to produce bottom-up via filling. The rotating ring-disk electrode (RRDE) is used to study the kinetic rate processes and additive transport under controlled conditions of convective-diffusion. These experimental studies were performed to understand the interactions of PEG, SPS, Cu (I), and oxygen using a rotating ring-disk electrode.

SPS by itself is likely not an accelerant, but a precursor. The actual accelerant probably is a Cu (I) thiolate formed when SPS reacts with Cu (I). Dissolved oxygen oxidizes Cu (I) to Cu (II). Hence, two competing reactions, one between Cu (I) and SPS, and one between Cu (I) and oxygen occur simultaneously. Under this hypothesis the oxygen concentration should influence the effectiveness of the accelerant. In these experiments, the working electrode, where plating takes place, is the ring, while the disk is used to generate Cu (I). The objective was to observe the response at the ring to Cu (I) generated at the disk and to correlate the response with oxygen and SPS concentrations and the rate of convective-diffusion.

1.2 Electrodeposition

The electrodeposition of metals involves heterogeneous charge transfer reactions and mass transport. For copper deposition, the reaction proceeds through two single-electron transfer steps.



The first step is kinetically slow, and requires a driving force of up to hundreds of millivolts. The second step is fast and is often assumed to be at equilibrium.

Transport of ions to the surface may also be rate-limiting. The transport of flux of species j , J_j is expressed in (1.3), and it includes diffusion, migration, and convection on the right-hand side (D_j : diffusion coefficient, C_j : concentration, z_j : charge number of the ion, F : Faraday's constant, ϕ : potential, v : velocity profile).

$$J_j = -D_j \nabla C_j - \frac{z_j F}{RT} D_j C_j \nabla \phi + C_j v \quad (1.3)$$

The potential where the net rate of reaction is zero is the open-circuit potential. If the reaction $\text{Cu (II)} \rightarrow \text{Cu (0)}$ is the only reaction allowed, the open-circuit potential is equal to the equilibrium potential, E_{eq} , of the $\text{Cu (II)} / \text{Cu (0)}$ couple. The surface overpotential, η_s , is defined as the difference between the actual potential and the equilibrium potential.

$$\eta_s = E - E_{eq} \quad (1.4)$$

For multiple reactions, such as anodic dissolution of copper to either Cu (I) or Cu (II) , the total current is the sum of partial currents.



$$I = I_I + I_{II} \quad (1.7)$$

The molar flux (N_i) of species is related to the partial current by Faraday's Law.

$$N_i = \frac{I_i}{nF} \quad (1.8)$$

1.3 Additives and current wave train in copper electrodeposition

The material used for via interconnections, copper, is a preferred metal because it fits the requirements of low resistance (16.78 n Ω -m @ 20°C), high allowed current density, and scalability. However, it is challenging to obtain a void-free filling inside a deep via by electroplating, especially with higher aspect ratio (ratio of depth to width up to 6 ~ 8). Voids and seams inside the vias (Figure 1.1) are common defects observed after copper electrodeposition because deposition is faster at the wafer surface than at the via bottom. In 1998, IBM demonstrated a profile evolution in wafer plating, described as superconformal (or superfilling) [1]. It is believed that additives and the applied current waveform are the key requirement for ideal filling by the copper electroplating process.

The addition of small amounts of certain substances changes the structures and properties of deposits. These additives can be classified as follows. [2-6]

- Levelers are used to suppress large-scale roughness. The coverage of leveler on concave areas is much less than on convex areas and therefore plating occurs preferentially on concave areas, producing a flatter surface. The concentration of levelers is typically 1~25 g/L, and they are usually nitrogen bearing organic compounds.
- Brighteners are used to suppress roughness at the micro level so that the roughness is smaller than the wavelength of light and the surface appears bright.

The concentration of brighteners is typically 0.005~4 g/L and they are usually sulfur bearing organic compounds.

- Wetting agents are used to lower the surface tension between air and the plating solution. They promote entry of the bath into vias as well as ejection of bubbles from the surface.

In the electronics industry, the most common plating baths for copper electrodeposition include acid sulfate baths and alkaline cyanide baths. Although acid sulfate baths provides slower deposition rates and rougher grain size compared to alkaline cyanide baths, the advantages of acid sulfate baths are less toxicity, simple components, almost 100% current efficiency, and cheaper operating cost. Therefore acid sulfate baths containing cupric sulfate and sulfuric acid are very popular. To achieve desired copper deposit characteristics, the selection of additives is important. In recent years, a great number of researchers have focused on polyethylene glycol (PEG) and bis-(3-sulfopropyl)-disulfide (SPS). PEG acts as a suppressor while SPS functions as an accelerant. It is believed that bottom up filling occurs when the accelerant accumulates at the via bottom and removes less strongly bound suppressors inside the vias. With the interactions of these additives, copper deposition in deep vias is possible.

The applied current waveform also plays an important role in the performance of deep via filling processes. Periodic pulse reverse (PPR) is a common method to plate copper in vias.

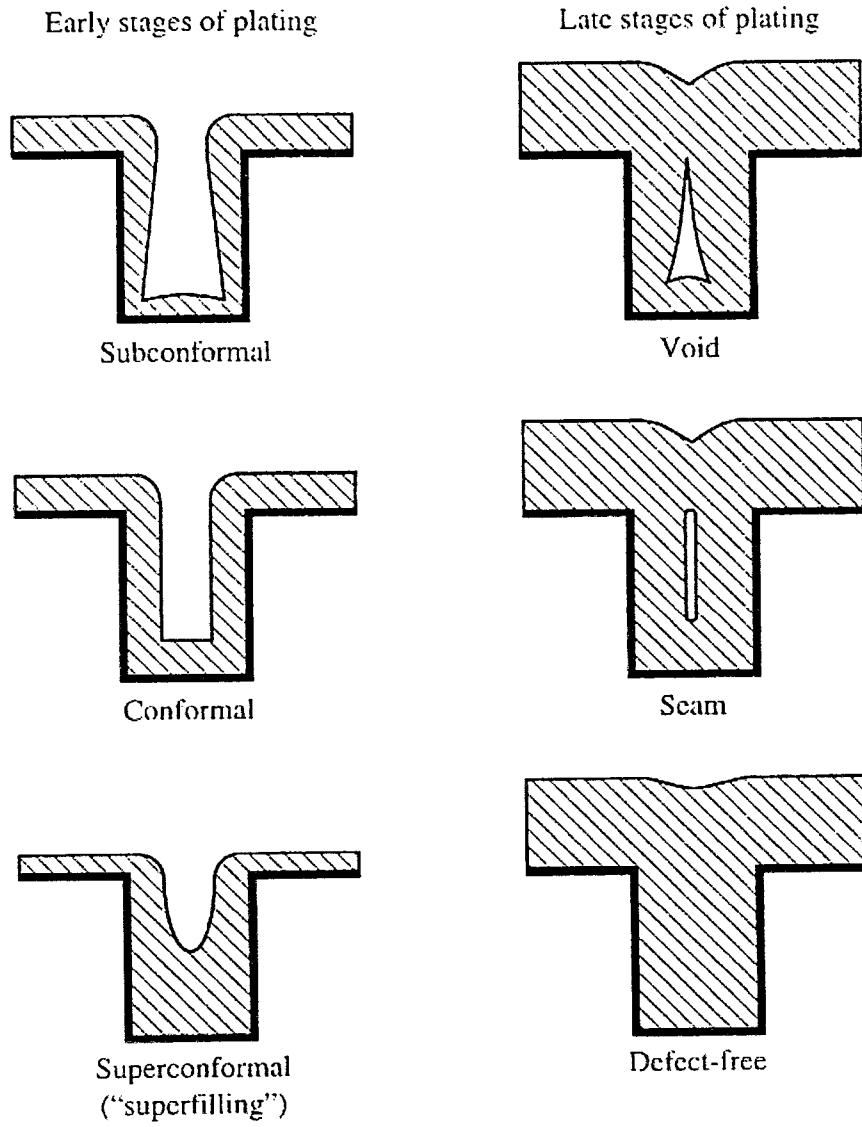


Figure 1.1 Types of profile evolution in via plating [1].

1.4 Rotating disk electrode and rotating ring-disk electrode

The rotating disk electrode (RDE) and rotating ring-disk electrode (RRDE) are used widely to perform analytical measurement of electrochemical reactions. Their structures are shown in Figure 1.2 [7]. The RDE consists of a disk electrode imbedded in a rod of an insulating material such as Teflon or epoxy resin. The rod is connected to a motor by a rotating shaft and rotated at a frequency f (revolutions per second). The rotation speed is the angular velocity, ω (1/s), where $\omega = 2\pi f$. For the RDE, the hydrodynamic equations for convective-diffusion have been solved under steady state conditions. When the reaction is under mass-transfer limitation, the Levich equation (1.9) defines the limiting current, i_l (A), where n is the number of electrons transferred in an electrode reaction, A is the area in cm^2 , D is the diffusion coefficient in cm^2/s , ν is the kinetic viscosity in cm^2/s , and C_0 is the bulk concentration in mol/cm^3 . The thickness of diffusion layer, δ (cm) is given by (1.10).

$$i_l = 0.62nFAD^{2/3}\omega^{1/2}\nu^{-1/6}C_0 \quad (1.9)$$

$$\delta = 1.61D^{1/3}\omega^{-1/2}\nu^{1/6} \quad (1.10)$$

The RRDE consists of a RDE with a second independently-controlled ring electrode concentric to the disk. Because fluid flows from the disk over the ring, material produced at the disk affects the ring reaction. For ring electrode with an inner radius r_2 and outer radius r_3 , the limiting current $i_{Ring,l}$ is given by (1.11)

$$i_{Ring,l} = 0.62nF\pi(r_3^3 - r_2^3)^{2/3}D^{2/3}\omega^{1/2}\nu^{-1/6}C_0 \quad (1.11)$$

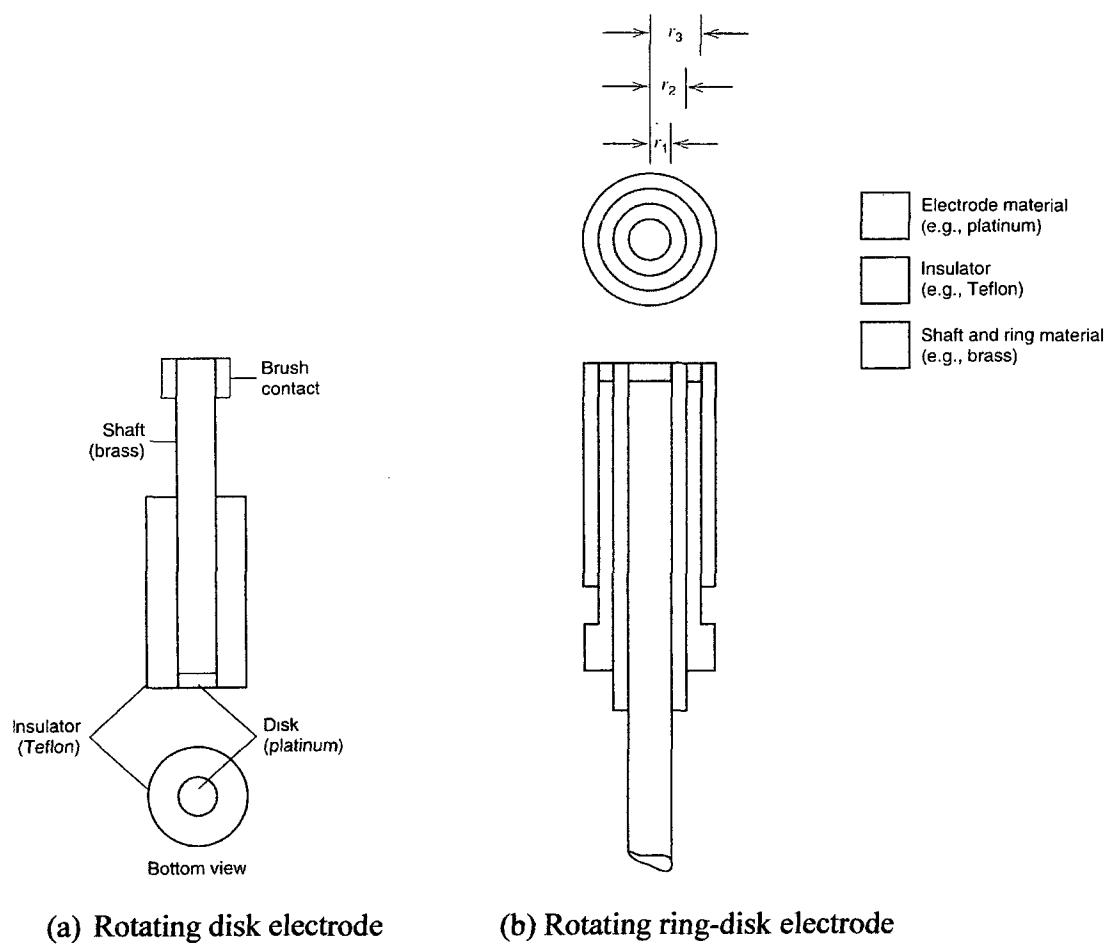
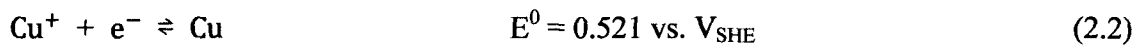
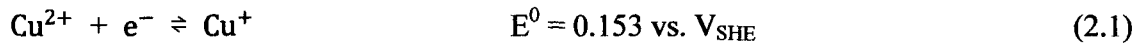


Figure 1.2 Structure of (a) rotating disk electrode and (b) rotating ring-disk electrode [7].

CHAPTER II: LITERATURE REVIEW

2.1 Copper electrodeposition and plating bath

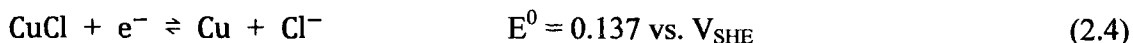
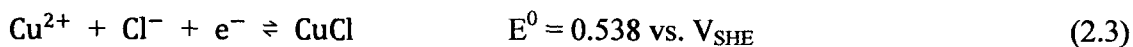
The cathodic deposition of copper in acid-sulfate solutions proceeds through two electron-transfer reaction in series.



(Standard hydrogen electrode, SHE, has all components at unit activity and the short-hand notation is Pt / H₂ (a=1) / H⁺ (a=1, aqueous)). The first reduction is much slower than the second one and therefore the rate determining step. In order to achieve the desired current distribution for copper electroplating inside small features, the addition of additives to control deposition kinetics is necessary. Acid-sulfur copper plating baths contain one or more additives including chloride, polyethylene glycol (PEG), and bis-(3-sulfopropyl)-disulfide (SPS). Among these additives, PEG is used as a suppressor to decrease the deposition rate, while SPS is used as an accelerant to increase the deposition rate. Competition between these effects at different locations inside the vias makes bottom-up deposition possible for via filling.

2.2 Effect of chloride

Chloride is one common component in copper plating baths. The presence of Cl⁻ results in the formation of CuCl, CuCl₂⁻, and CuCl₃²⁻. Depending on Cl⁻ concentration and potential, a CuCl monolayer may be generated at the electrode surface and then reduced by the following reactions [8].



Due to the low solubility of CuCl in the plating bath, a film may form at Cl⁻ concentrations of 30 mg/L to 40 mg/L [9].

The CuCl monolayer mediates copper deposition and accelerates the overall reduction process. Low (few mM) or high (M) levels of Cl⁻ concentration also influence copper deposition through two competitive effects [10]. Cl⁻ depolarizes the copper reduction process at low concentration. Complexation consumes free cupric ions and results in cathodic polarization of the reduction process at high concentration.

2.3 Effect of polyethylene glycol

Polyethylene glycol (PEG) is a polymer with the structure HO-(CH₂-CH₂-O)_n-H. It has been established that addition of PEG into copper electrolytes increases overpotential and decreases deposition rate. It is believed that polyether macromolecules are absorbed on the growing surface and impede copper deposition. Stoychev et al. found that complexation of PEG with Cu (I) and/or Cu (II) enables adsorption [11]. Copper ions are moderate acids and react with oxygen containing molecules. Thus, the ethylene oxide ligand complexes with copper ions and blocks the transfer of copper ions from the solution to the surface of the metal.

In recent years, the researchers have showed that PEG may be adsorbed in different forms such as monolayer, multi-layer film, rod-like PEG molecules, and spherical PEG molecules. The forms also depend on potential [11-13]. The study by Healy et al. with Raman spectroscopy and electrochemical measurements [14, 15] shows that a simple

neutral PEG is adsorbed at negative potential with the copper chloride complexing with PEG as a ligand. However, some studies show that PEG by itself in the bath has only a small effect on the deposition kinetics [12, 13]. This is supported by slight adsorption of PEG on copper surface in sulfuric electrolyte [16] and weak adsorption of PEG macromolecules on steel during copper plating [17]. Although there are contradictory explanations about the adsorption of PEG, it is certain that the combination of PEG and Cl^- synergistically suppress copper electrodeposition.

The study of additives on polarization behavior by Kelly et al. [12] shows that Cl^- alone in the bath promotes copper deposition while PEG alone has little suppression effect, (Figure 2.1). The addition of PEG and Cl^- produces significant inhibition and increases over-potential. This explains why PEG adsorbed on copper with Cl^- adopts the spherical conformation shown in Figure 2.2. Here, Cu (I) serves as an intermediate to link PEG and Cl^- . Each Cu (I) associates with six oxygen atoms of the polyethylene oxide chains to form a positively charged complex. Because of the positive charge, Cl^- is attracted to the complex and adsorbs on the copper surface. At cathodic potentials, the Cu (I)-oxygen bond breaks, liberating Cu (I) ions, reducing Cu (I) to Cu, and returning PEG to the bulk solution [11]. The reactions are shown as below [18].

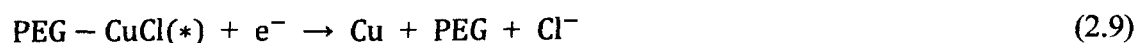
PEG surface adsorption:



Surface adsorbed PEG-CuCl complex:



Final reduction:



Dow et al. believe that Cl^- acts as a dynamic anchor to immobilize the PEG-Cu (I)- Cl^- complexes onto the as-deposited copper and the binding strength between Cl^- and the PEG is related to the number of ether groups in the PEG (Figure 2.3) [19]. Thus, PEG with smaller molecule weight links fewer Cl^- , and provides weak adsorption and weak suppression. Their results show that PEG with molecule weight ranging from 6000 to 8000 g/mol would obtain the best via filling performance (Figure 2.4).

Increasing the PEG concentration at fixed Cl^- concentration was observed to enhance suppression. On the other hand, increasing Cl^- concentration at fixed PEG concentration also enhances inhibition. However, once the Cl^- concentration is too high, this synergetic interaction no longer exists and the deposition rate becomes isotropic [20]. According to the model to predict steady-state current-potential curves during deposition for Cl^- concentrations from 10^{-3} (0.036 ppm) to 1 mM (36 ppm), the minimum Cl^- concentration to suppress copper deposition through the entire potential range is about 1mM (36 ppm) [21].

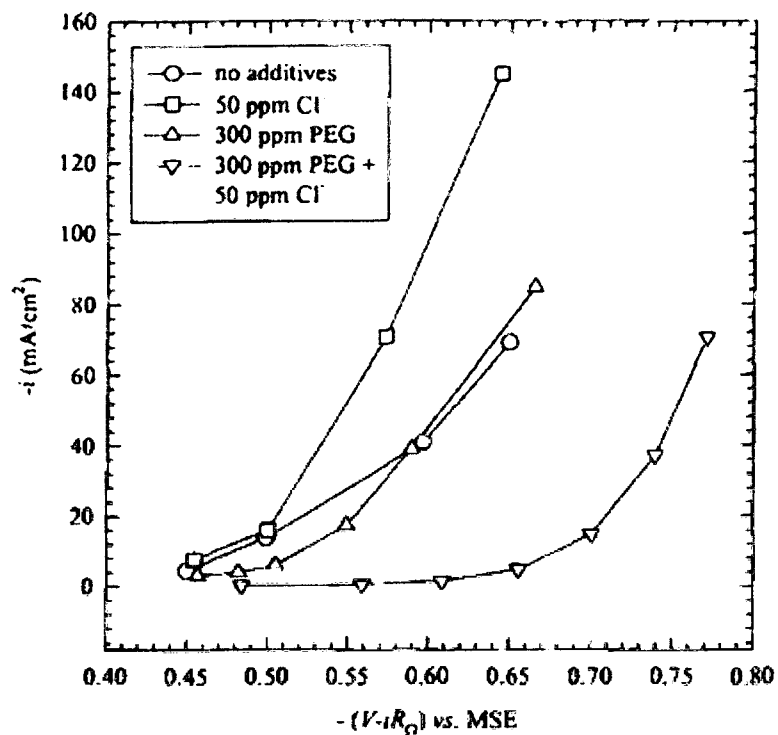


Figure 2.1 Effect of PEG and Cl⁻ on the polarization behavior through RDE at 900 rpm [12].

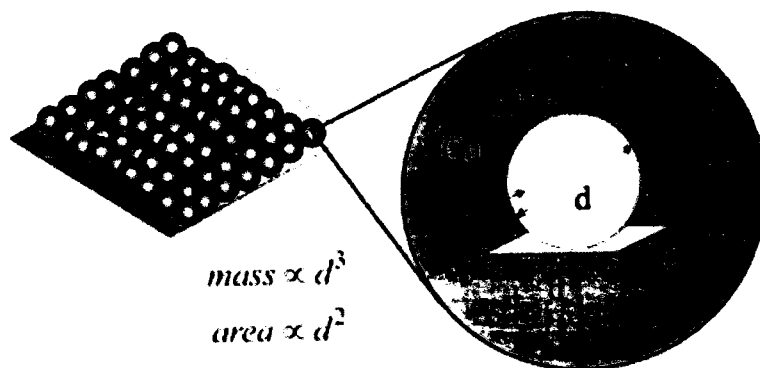


Figure 2.2 Adsorption of spherical PEG molecules on copper [12].

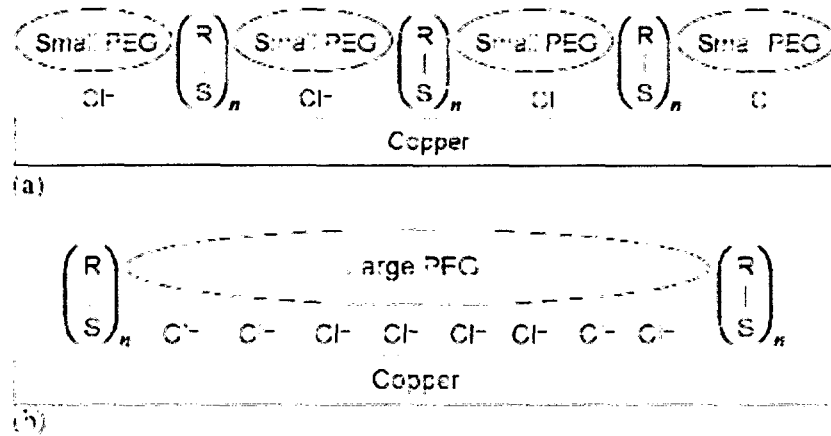


Figure 2.3 Illustration of synergetic adsorption of PEG and Cl⁻; (R-S) represents (CH₂)₃-SO₃⁻, (a) Smaller PEG molecule weight (b) Larger PEG molecule weight [19].

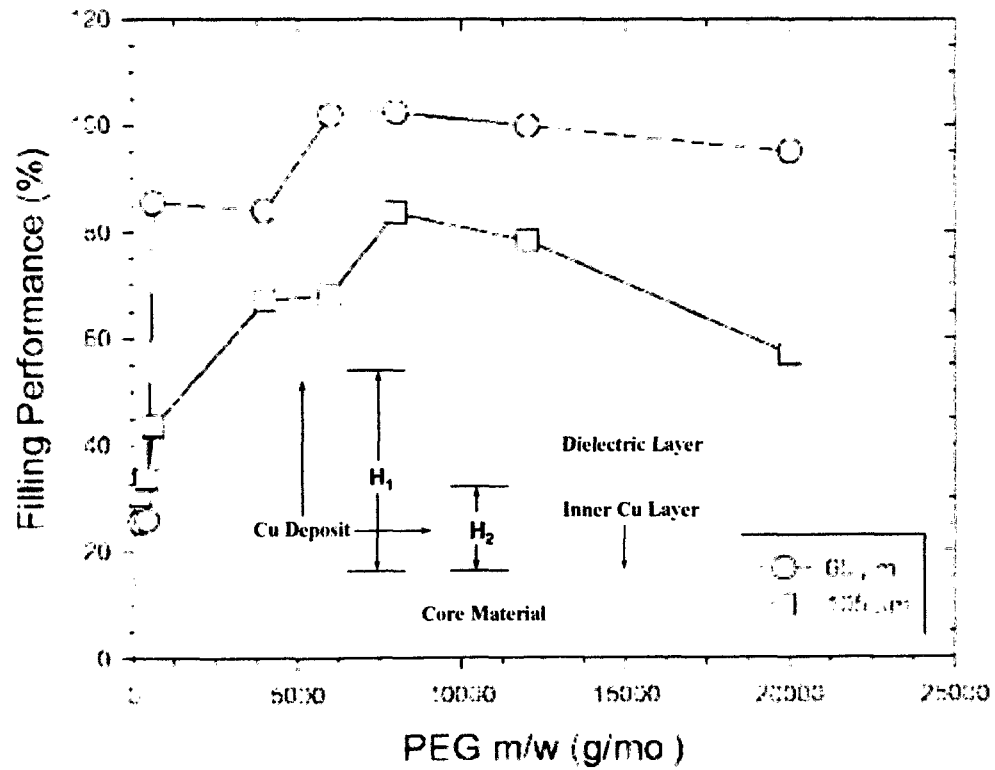


Figure 2.4 Filling performance as a function of PEG molecule weight. Via diameters are (○) 65 μm and (□) 105 μm. Via depth is 55 μm. The definition of filling performance is given by $(H_2/H_1) \times 100\%$ [19].

2.4 Effect of bis-(3-sulfopropyl)-disulfide

Bis-(3-sulfopropyl)-disulfide, SPS, is commonly used as an accelerant. Its derivative, 3-mercaptopropyl sulfonate, MPS, has also been widely studied. The chemical structures are shown in Figure 2.5.

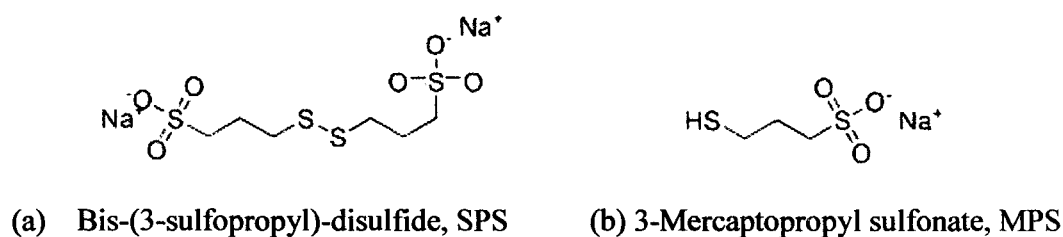
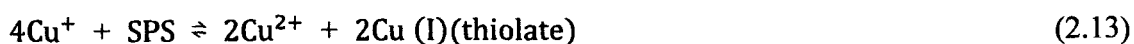
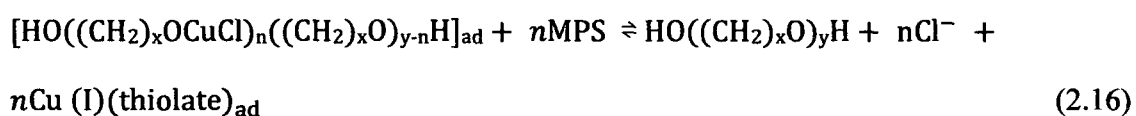
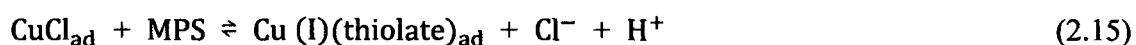


Figure 2.5 Chemical structures of (a) SPS, and (b) MPS

SPS by itself is a mild inhibitor. According to Hung et al. [22], addition of SPS at 10 ppm concentration without PEG in copper electrolyte inhibits the electroplating rate. According to a study by Kondo, the acceleration of copper deposition results from the accumulation of Cu (I)(thiolate) and the related reactions shown as below [23-25]. It is important that SPS by itself cannot reduce Cu (II) to Cu (I). First it has to be reduced to MPS by reaction (2.10). When SPS concentration is too low, the formation of Cu (I)(thiolate) is too slow to accelerate the deposition rate. However, the acceleration on copper deposition is observed when SPS concentration is raised to 100 ppm and reaches a limit at 1000 ppm.



Cu (I) ions form complexes with Cl^- , and then further react with MPS. The higher complexation reactions are shown as reactions (2.5) and (2.15). These adsorbed species (subscript as “ad”) formed on the surface interact with the bulk solution, and therefore ligands can be exchanged. For example, reaction (2.16) shows the displacement of PEG-CuCl complexes by Cu (I)(thiolate), which demonstrates the chemical equivalent of competitive absorption between the suppressor and accelerant [25].



In the PEG-SPS- Cl^- system, the addition of SPS to the electrolyte results in a strong influence on deposition rate. Moffat et al. measured potential versus current curves (Figure 2.6) at SPS concentrations ranging from 0.17 $\mu\text{mol/L}$ (0.3 ppm) to 499 $\mu\text{mol/L}$ (176 ppm) [26]. They explain that the acceleration effect results from the disruption and/or displacement of the passivating PEG-CuCl complexes, and this competitive adsorption depends on the thiol or sulfonate end groups of the accelerant. Tan et al. studied the influence of end groups on MPS, 1, 3-propanedithiol (PDT) and 1, 3-propanedisulfonic (PDSA), where MPS has one thiol and one sulfonate end group, PDT has two thiol end groups, and PDSA has two sulfonate end groups [27]. The result (Figure 2.7) shows the synergetic acceleration of PDSA and Cl^- , but inhibition effect from MPS or PDSA, which demonstrates the sulfonate group is responsible for acceleration in the presence of chloride.

The potential dependent behaviors of PEG-SPS- Cl^- and PEG-MPS- Cl^- has also been

extensively studied [27, 28]. Figure 2.8 shows a comparison of two systems. A similar acceleration effect can be observed with 5 ppm SPS and 0.5 ppm MPS as applied high overpotential ($-0.75 V_{SSE}$). At lower overpotential ($-0.5 V_{SSE}$), the acceleration effect of SPS (5 ppm or 50 ppm) is smaller than that of MPS. This result demonstrates that the effectiveness of SPS is highly dependent on applied potential while that of MPS is less sensitive to applied potential. Possible explanations include potential dependent reduction from SPS to MPS, and the fact that acceleration happens through an MPS pathway.

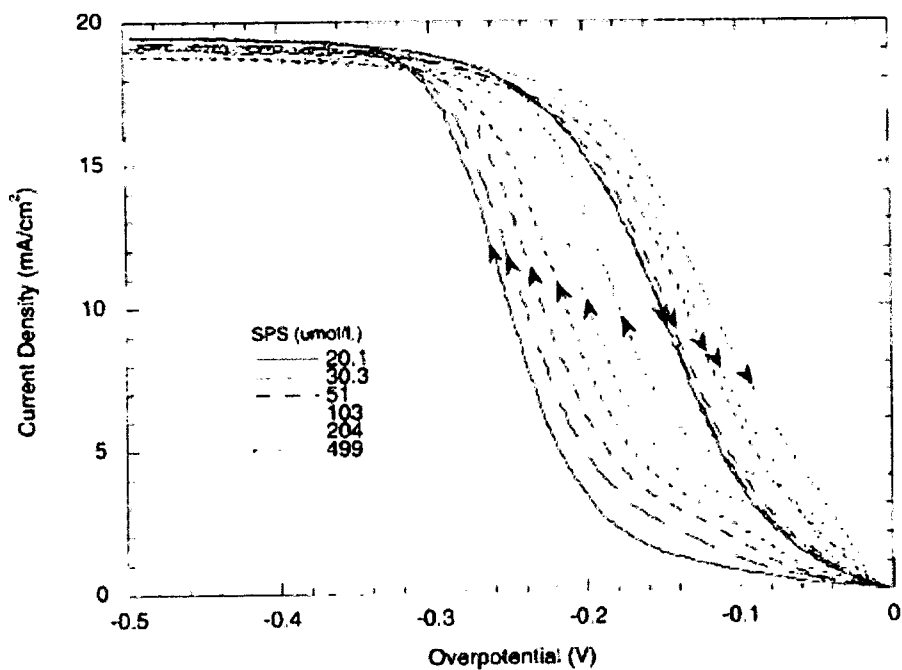
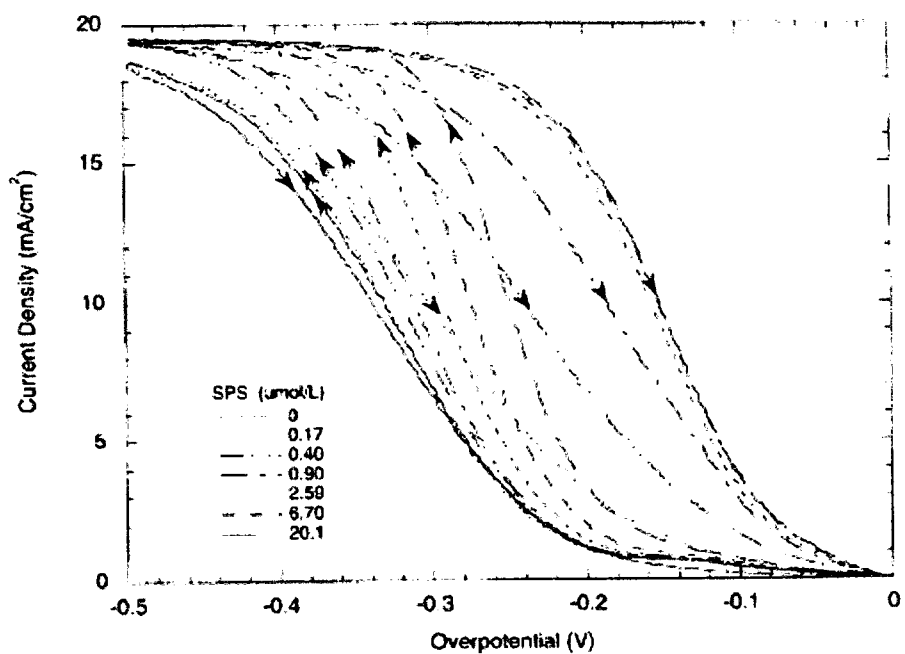


Figure 2.6 Hysteric η - i curves with various SPS concentrations in the presence of PEG and Cl^- additives. Top: 0 ~ 20.1 $\mu\text{mol/L}$ SPS; bottom: 20.1 ~ 499 $\mu\text{mol/L}$ SPS [26].

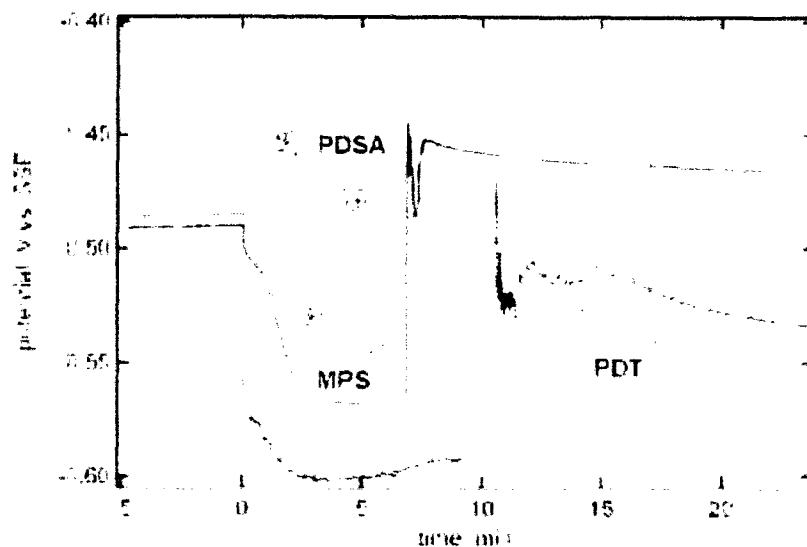


Figure 2.7 Behavior of MPS, PDT, and PDSA at 1 ppm when added to the basic electrolyte. The upward step change in the potential comes from the addition of chloride [27].

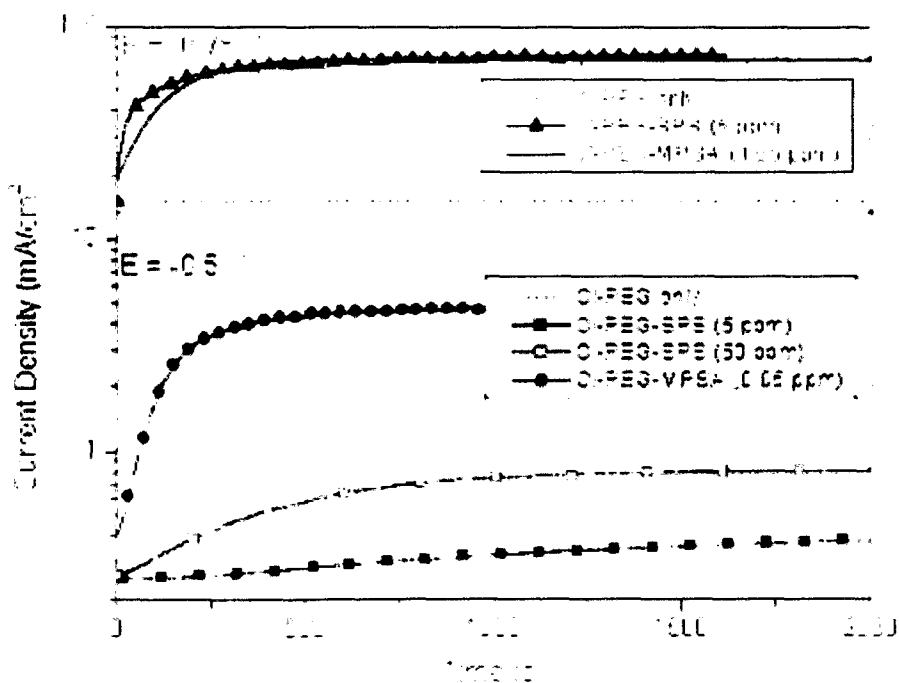


Figure 2.8 Potentiostatic behavior of PEG-SPS-Cl⁻ and PEG-MPS-Cl⁻ systems. Basic electrolyte with 50 ppm Cl⁻, 300 ppm PEG, and 5 ppm SPS / 0.05 ppm MPS [27].

2.5 Mechanisms of via filling

Since IBM introduced the idea of superconformal deposition [1] of copper for on-chip interconnects in 1998, its mechanism has been widely explored and developed. Early modeling describes a location dependent mechanism resulting from diffusion limited consumption of the inhibitor inside the trenches. However, this model seems to be insufficient to fit vias with higher aspect ratio today.

The curvature enhanced accelerator coverage (CEAC) mechanism provided by Moffat and Wheeler et al. describes competitive adsorption between accelerator and suppressor [28]. Inside the vias, the accelerator removes the less strongly bound suppressor, and the accumulation of the adsorbed accelerator arises to higher local deposition rate, which provides bottom-up filling.

However, the model is based on a steady state additive flux arriving at the bottom of the vias. A series of experiments on transient polarization response with injection of various additive mixtures into plating bath obtained the following conclusions [29]. PEG adsorbs almost instantaneously on the additive-free copper surface. However, PEG cannot adsorb on the SPS-covered electrode. Moreover, the diffusion of PEG is slower ($D \sim 5 \times 10^{-7} \text{ cm}^2/\text{s}$). On the other hand, SPS adsorbs moderately fast (slower than PEG) on the additive-free surface, but adsorbs slowly on PEG-covered surface. In addition, SPS diffuses faster ($D \sim 10^{-5} \text{ cm}^2/\text{s}$).

The transient additives interactions are illustrated by Akolkar et al. as Figure 2.9. (a) $t = 0$, the additives in the bulk solution enter the vias by capillary force. (b) $t < 1\text{s}$, the characteristic of fast adsorption but slower diffusion makes most of the PEG instantaneously adsorb along with the rim and sidewall of vias, and the inhibition of PEG is limited by diffusion control. (c) $t = 1\text{s}$, fast diffusion of SPS arrives as the via bottom

and adsorbs on the PEG-free surface, which is controlled by adsorption kinetics. (d) $t = 10$ s, the bottom is accelerated by SPS while the sidewall is inhibited by PEG. In addition, the same authors also model the location-dependent deposition rate, which is affected by not only the transport-adsorption process but local surface area reduction. The area reduction provides more SPS coverage and thus enhances acceleration. They conclude that the transport-adsorption process dominates with the via aspect ratio ≥ 20 while the transport-adsorption time scale is negligible compared to via-fill duration with the vias aspect ratio ≤ 4 . At the intermediate aspect ratio, both transport-adsorption process and local surface area reduction effects are important [30].

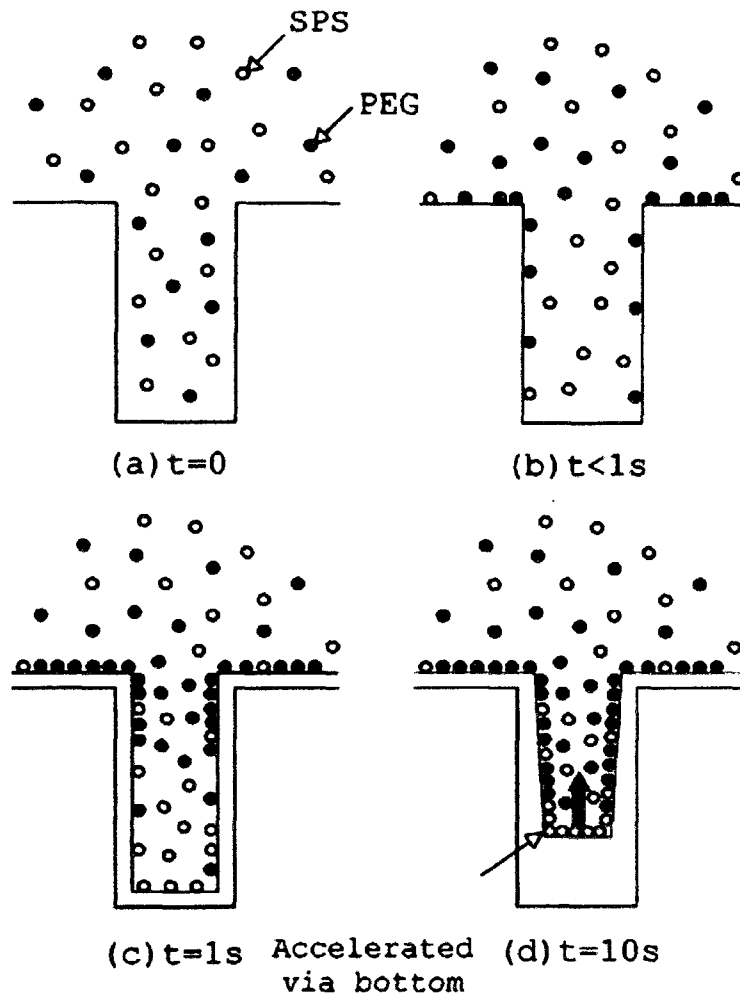
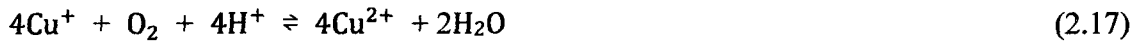


Figure 2.9 Model for transient additive interactions during the bottom-up fill of high aspect ratio vias. (a) $t = 0$, additives diffuse into the via. (b) $t < 1$ s, Fast PEG adsorption on the sidewall causes suppression. (c) $t = 1$ s, Fast SPS diffuses into the bottom and adsorbs on the PEG-free surface. (d) $t = 10$ s, Acceleration on the bottom and suppression on the sidewall. Not drawn to scale [29].

2.6 Via filling with oxygen purging

The acceleration effect of dissolved O_2 was investigated by Kondo et al. [31] which provides another pathway to via filling. With O_2 purge, Cu (I) is consumed. Related reactions are shown as follows and illustrated in Figure 2.10 [23].



More oxygen is present outside the vias than inside the vias, and thus more Cu (I) (thiolate) outside the vias is oxidized to Cu (II), where inhibition is stronger. On the other hand, the via bottom with less oxygen arriving accumulates more Cu (I) (thiolate) accelerant and gives rise to acceleration. This two effects by different Cu (I) (thiolate) accumulation result in the superconformal structure [1]. The result is shown in Figure 2.11.

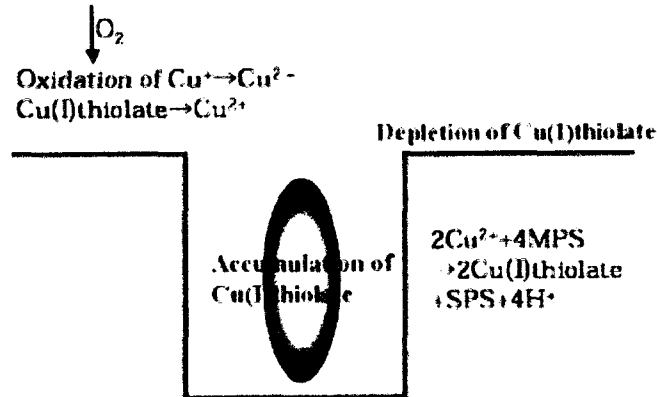


Figure 2.10 Schematic of via filling with dissolved oxygen [23].

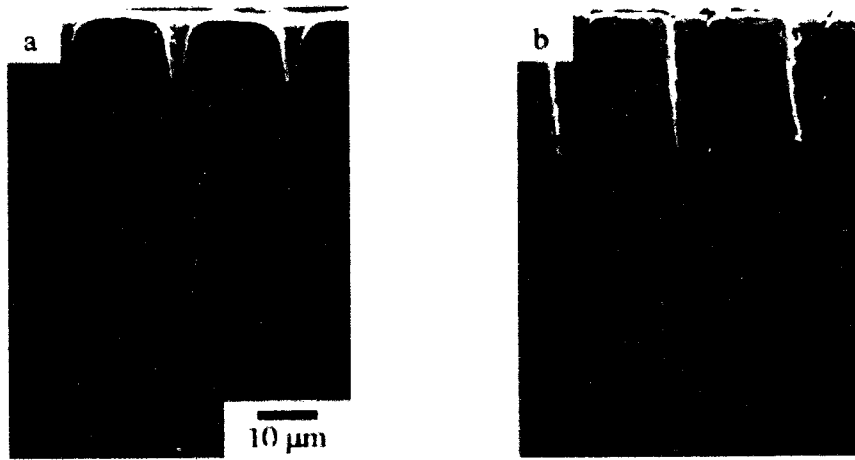


Figure 2.11 Micrographs of via cross section in two-stage plating process without and with O₂ purging. (a) without O₂ purging; (b) with O₂ purging [23].

CHAPTER III: EXPERIMENTAL

3.1 Introduction

A rotating ring-disk electrode was used to study the interactions among PEG, SPS, Cu (I) and oxygen. By variation of rotation speed or stripping potential at the disk, the generation of Cu (I) from the disk can be varied. The Cu (I) generated at the disk then takes part in competing reactions with oxygen or SPS before reaching the ring. These reaction diffusion processes can be carried out under various conditions through control of the SPS and dissolved oxygen concentrations and the flow rate from disk to ring.

3.1.1 Reaction diffusion model

This experiment is based on the model of filling illustrated in Fig 2.10. Cu (I) reacts with SPS and generates the accelerant, Cu (I) (thiolate), both at the surface and the bottom of vias. The Cu (I) at the via surface is consumed by oxygen while the Cu (I) at the via bottom where there is less oxygen is consumed more slowly. Therefore, more accelerant is generated inside the via, resulting in faster Cu deposition at the bottom than the surface. The rotating ring-disk electrode is adopted to simulate the mechanism. In this experiment, the disk first plated with copper and then subjected to a positive potential to generate Cu (I). The Cu (I) reacts with SPS to form accelerant which is advected to the ring. The ring is held at a negative potential to deposit Cu.

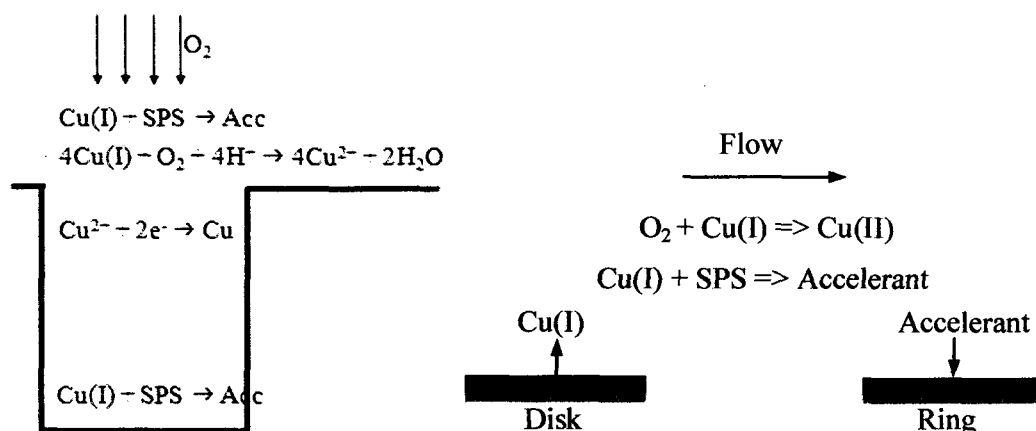
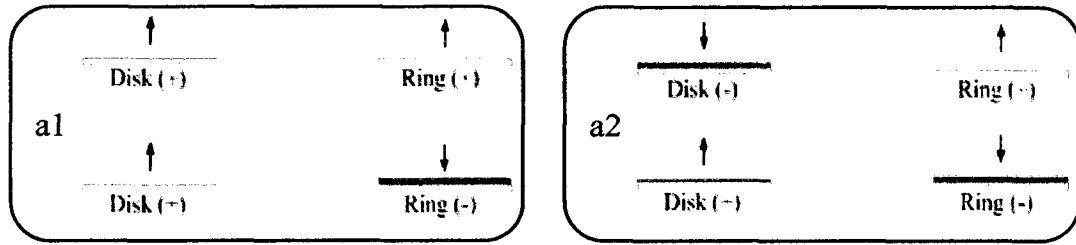


Figure 3.1 Left: bottom-up filling with O_2 purging. Right: Simulated interactions at a RRDE with deposition on the ring and concurrent stripping on the disk.

The objective is to observe the response at the ring to Cu (I) generated at the disk and to correlate the response with the Cu (I) reaction-diffusion processes. The experiment consists of a sequence of four procedures termed a1, a2, b1, and b2. In procedure a1, a positive potential is applied to both disk and ring for period of 5 seconds, then a negative potential is applied to the ring while the disk is held at a positive potential for the period of 20 seconds. In procedure a2, the disk is held at a negative potential for 5 seconds, causing deposition of copper on the disk. This copper is then stripped while Cu is deposited at the ring. The first step in a1 cleans both electrodes. The second provides the ring deposition rate when no Cu (I) is being generated at the disk. The first step in a2 charges the disk with copper. The second provides the ring deposition current when Cu (I) is being generated at the disk.



(a) a1 procedure

(b) a2 procedure

Figure 3.2 Cu deposition on the ring without and with Cu (I) generation on the disk

Dissolution of copper from the disk proceeds through the parallel processes:



The ratio of Cu (I) partial current to total current is measured by the procedures shown in Fig 3.3. The deposition and stripping potential in procedures b1 and b2 is the same at initial and second steps in the a2 procedure, but the ring is inactive. Combined with the derivation shown as below, the Cu (I) partial current could be calculated from deposit charge ($Q_{Deposit}$) and stripping charge (Q_{Strip}) according to molar flux balance. Q^I and Q^{II} stand for the charges of Cu (I) and Cu (II) generation at the disk.

$$\frac{Q_{Deposit}}{2} = Q^I + \frac{Q^{II}}{2} = \frac{Q^I}{2} + \frac{Q^I + Q^{II}}{2} \quad (3.8)$$

Therefore (3.8) becomes

$$\frac{Q_{Deposit}}{2} = \frac{Q^I}{2} + \frac{Q_{Strip}}{2} \quad (3.9)$$

Divided by $\frac{Q_{Strip}}{2}$ on both sides to give

$$\frac{Q_{Deposit}}{Q_{Strip}} = \frac{Q^I}{Q_{Strip}} + 1 \quad (3.10)$$

The desired expression of Cu (I) becomes

$$Cu(I) = \frac{Q'}{Q_{Strip}} = \frac{Q_{Deposit}}{Q_{Strip}} - 1 = \frac{Q_{Deposit} - Q_{Strip}}{Q_{Strip}} \quad (3.11)$$

$$Cu(I)\% = \frac{Q_{Deposit} - Q_{Strip}}{Q_{Strip}} \times 100\% \quad (3.12)$$

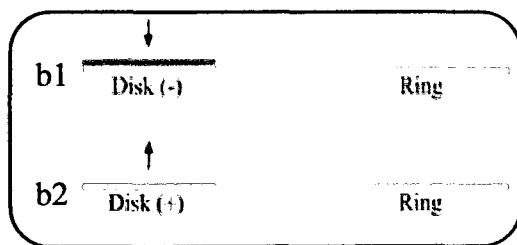


Figure 3.3 Cu deposition and stripping in procedure b1 and b2.

3.2 Experimental setup and instrumentation

3.2.1 Electroplating cell

A small reaction vessel with two 14/20 side necks was used. Solution volumes as small as 10 ml for were used in the experiments. A three-electrode arrangement was used for all experiments. The reference electrode was a Teflon-insulated copper wire cut to expose the end and the counter electrode was also a copper wire. The working electrode is a PINE instrument rotating ring-disk electrode and its disk outer diameter, ring inner diameter and ring outer diameter are 4.57 mm, 4.93 mm, and 5.38mm, respectively. The collection efficiency of the RRDE is about 22% where the collection efficiency is used to correlate the ring current and the disk current, and it only depends on disk outer diameter, ring inner diameter and ring outer diameter. The rotating ring-disk electrode was inserted in the center neck. The use of the two side necks allowed the reference and counter electrodes to be closer to working electrode to decrease the resistivity from electroplating solution.



(a) ACE GLASS Reaction Vessel



(b) PINE Rotating Ring-Disk Electrode

Figure 3.4 Electroplating cell and electrode

3.2.2 Bipotentiostat and modulated speed rotator

The experiment requires a bi-potentiostat to control the potential and to measure current responses of the disk and ring during the reaction. All the experiments were performed using a bipotentiostat (PINE AFCBP1) controlled by a PC. In addition, a modulated speed rotator (PINE AFMSRX) was used to control the rotation speed of the RRDE.

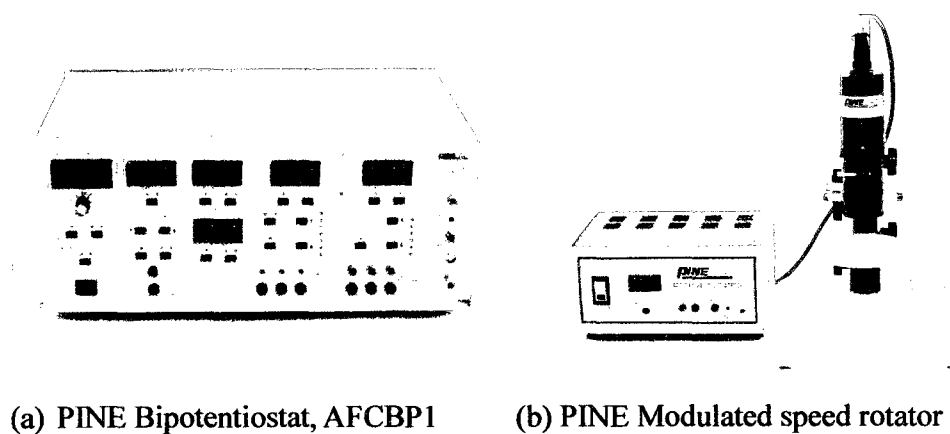


Figure 3.5 Bipotentiostat and modulated speed rotator

3.2.3 Chemical reagents

The base solution was 0.6 M CuSO₄ and 1.0 M H₂SO₄. Hydrated cupric sulfate with molecule weight 249.68 (J. T. Baker) and 96% concentrated sulfuric acid (J. T. Baker) was used to make up the solution. The PEG-SPS-Cl⁻ additive system was used and the components are shown in Table 3.1. Sodium chloride (J. T. Baker) with molecule weight 58.44, PEG 6000 (EMD), and SPS (Raschig GmbH) were used for additives.

Table 3.1 Copper electroplating solution components

Item	Component	Concentration	
1	Cupric sulfate pentahydrate	CuSO ₄ · 5H ₂ O	0.6 M
2	Sulfuric acid	H ₂ SO ₄	1.0 M
3	Chloride	Cl ⁻	50 ppm
4	Polyethylene glycol 6000, PEG	HO-(CH ₂ -CH ₂ -O) _n -OH	400 ppm
5	Bis-(3-sulfopropyl)-disulfide, SPS	C ₆ H ₁₀ Na ₂ O ₆ S ₄	Varied

3.2.4 Experimental matrix

The experiments were based on three independent variables: SPS concentration, rotation speed, and disk-stripping-potential. The concentrations of each component except SPS were the same in each experiment. The SPS concentration was varied from 0 to 40 ppm. The RRDE rotation speed was varied from 5 to 400 rpm. The stripping potential was varied from 50 to 300 mV. In addition, the experiments were repeated under three atmospheres: air, oxygen, and argon. Some experiments were also run without additives (SPS and PEG) for comparison with additive experiments.

Table 3.2 Experimental matrix

Cell	Effect	[SPS]	Rotation Speed	Stripping Potential
1		0 ppm	100 rpm	200 mV
2		4 ppm	100 rpm	200 mV
3	SPS concentration	10 ppm	100 rpm	200 mV
4		20 ppm	100 rpm	200 mV
5		40 ppm	100 rpm	200 mV
6		10 ppm	5 rpm	200 mV
7		10 ppm	10 rpm	200 mV
8	Rotation speed	10 ppm	25 rpm	200 mV
9		10 ppm	100 rpm	200 mV
10		10 ppm	225 rpm	200 mV
11		10 ppm	400 rpm	200 mV
12			10 ppm	100 rpm
13		10 ppm	100 rpm	100 mV
14	Disk-stripping-potential	10 ppm	100 rpm	150 mV
15		10 ppm	100 rpm	200 mV
16		10 ppm	100 rpm	250 mV
17		10 ppm	100 rpm	300 mV

CHAPTER IV: RESULTS AND DISCUSSION

4.1 Effect of SPS concentration

In these measurements, the concentrations of PEG and Cl^- were held at 400 ppm and 50 ppm respectively while the SPS concentration was varied from 0 to 40 ppm. The experiments were repeated under air, oxygen and argon atmospheres. In each set of experiments, a series of procedures was applied to the rotating ring-disk electrode. The parameters are shown in Table 4.1. 10 consecutive runs were performed under each condition. For procedure a1 and a2, both disk and ring are stripped at 600 mV potential to remove all copper from the electrode surface before the next run.

Table 4.1 Bipotentiostat parameters of a1, a2, b1, and b2 procedures

Procedure	Step	Disk potential, Φ_D	Ring potential, Φ_R
a1	Initial (5 sec)	200 mV	200 mV
	Experiment (20 sec)	200 mV	-300 mV
a2	Initial (5 sec)	-250 mV	200 mV
	Experiment (20 sec)	200 mV	-300 mV
b1	Initial (5 sec)	0 mV	-
	Experiment (20 sec)	-250 mV	-
b2	Initial (5 sec)	0 mV	-
	Experiment (20 sec)	200 mV	-

4.1.1 Ring current transients under air

The experiment was first carried out with no SPS in the solution (see Figure 4.1a). First procedure a1, without disk stripping, was applied. In the presence of PEG and Cl^- , a PEG-Cu (I)- Cl^- complex suppresses the ring deposition current. In consecutive runs, the inhibition effect increased from run to run until it reached a saturated level with continuous runs. Figure 4.1b shows the ring deposition current with copper stripping from the disk (procedure a2). Similarly, the suppression effect occurs on the disk and the ring electrodes. The time-integrated disk stripping current shows that less copper is stripped with each consecutive run. However, the current at the ring seemed to be less sensitive to the inhibition effect. It is clear that generation of Cu (I) at the disk does not influence the inhibition at the ring, and the suppression has reached certain level of saturation.

10 ppm SPS was then added to the bath with fixed concentrations of other components. The ring current transients without and with copper stripping at the disk are shown in Figure 4.2. Accelerated ring-current transients are observed both with and without Cu (I) generation at the disk. In addition, a peak occurs from 0.4 ~ 2.8 seconds during disk stripping (Figure 4.2b), meaning a sudden kinetic acceleration causes the increase of current. After about 3 seconds of disk-stripping, the ring current drops to a plateau. Cu (I) transported by convective diffusion from the disk reacts to form the accelerant and produces acceleration. Comparison of ring current transients on the 10th run is shown for varied concentrations of SPS in Figure 4.3. The current is almost unchanged with 0 ppm SPS while the current is increased with more SPS. Furthermore, higher and longer acceleration appears with more SPS concentration up to 40 ppm. Although the trend of ring current from a1 to a2 is increased in general, it shows a drastic

raise with SPS of 4 ~10 ppm, and less increase with additional SPS, meaning a gradually saturated acceleration of copper deposition.

In Figure 4.4, the charge in each run is calculated from the time-integrated current as a function of run number with SPS concentration from 0 ppm to 40 ppm. Accordingly, the more stable charge (after 5th run) is almost unchanged from a1 to a2 for SPS = 0 ppm while it increases from a1 to a2 for SPS \geq 4 ppm. However, a saturated acceleration with more SPS also aligns with the result in Figure 4.3. A possible reason for the saturated acceleration may result from the limited Cu (I) concentration, whatever originally existing in the bath or generating from the disk, insufficient to react with more SPS and producing more accelerant.

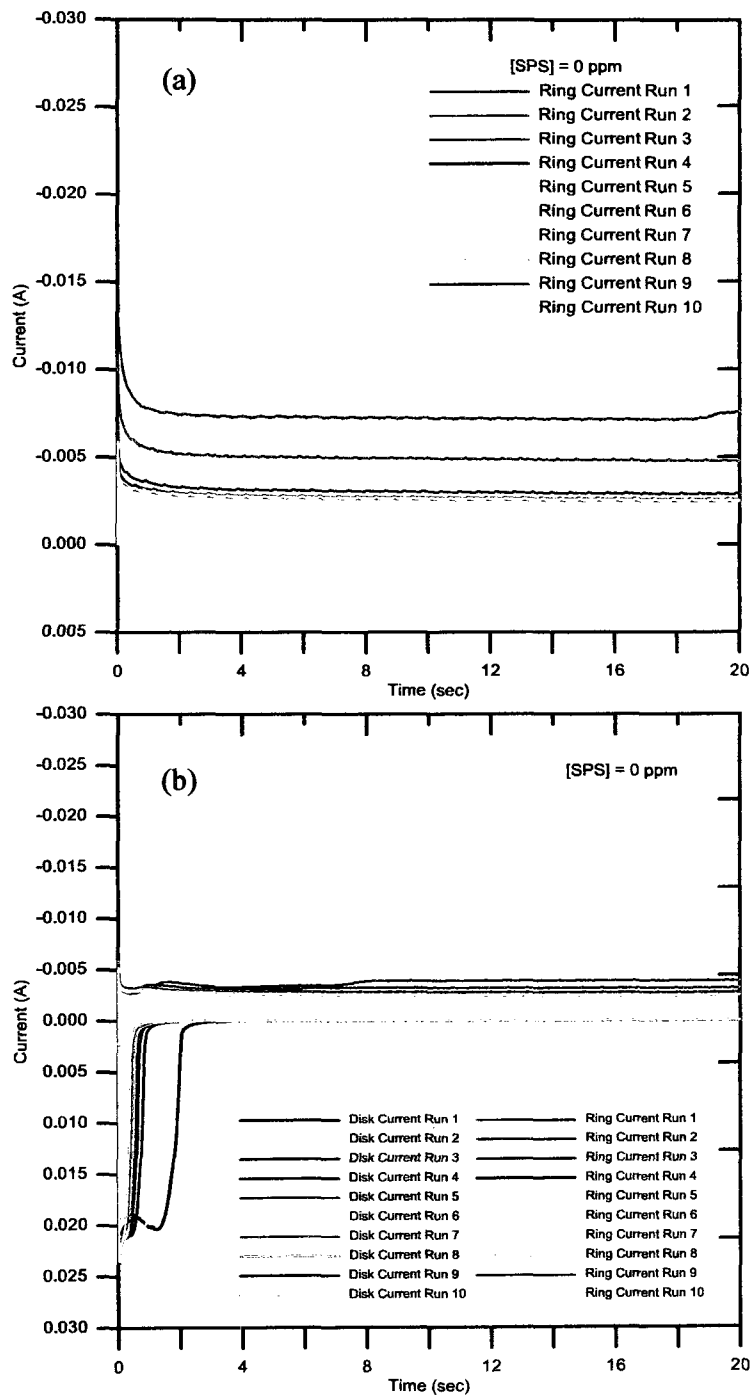


Figure 4.1 Ring current transients under air, (a) without Cu (I) generation at the disk, (b): with Cu (I) generation at the disk. [PEG] = 400 ppm, [SPS] = 0 ppm, $\omega = 100$ rpm, $\Phi_D = 200$ mV.

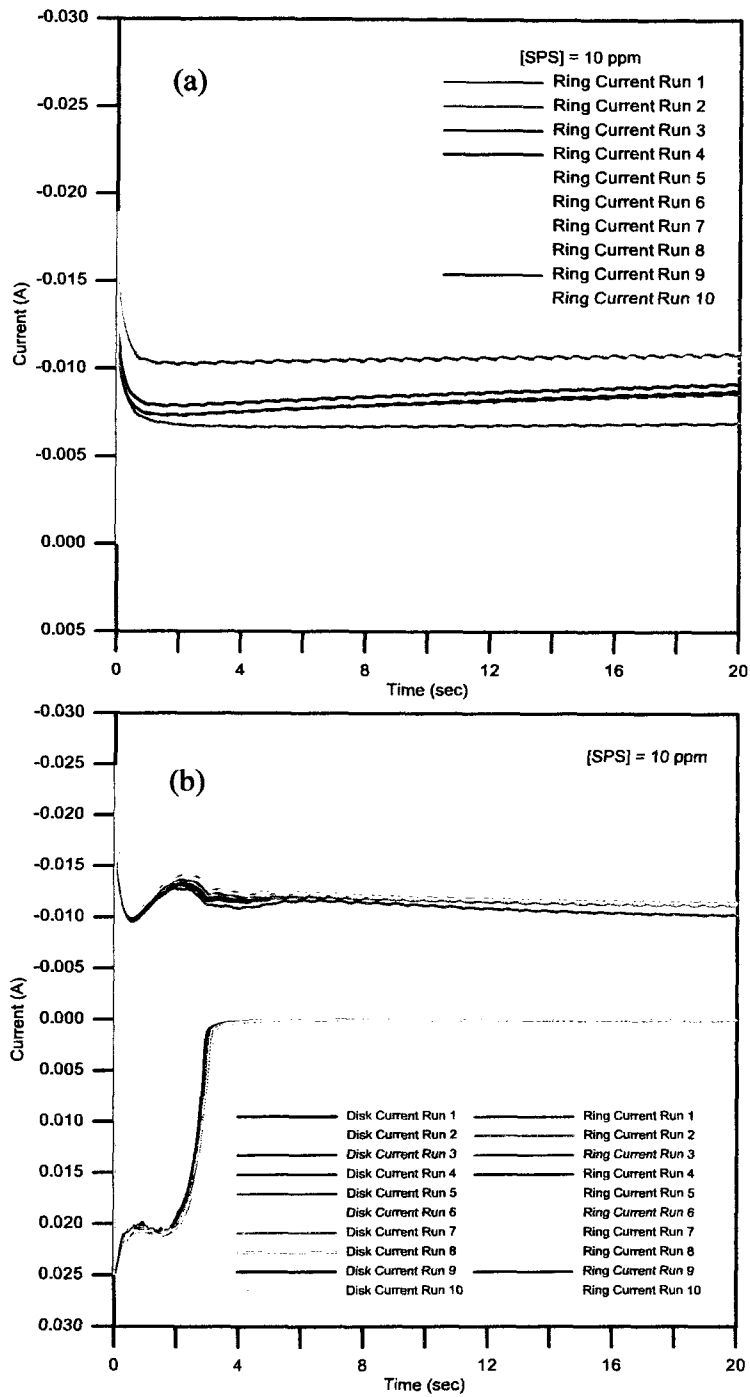


Figure 4.2 Ring current transients under air, (a) without Cu (I) generation at the disk, (b) with Cu (I) generation at the disk. [PEG] = 400 ppm, [SPS] = 10 ppm, $\omega = 100$ rpm, $\Phi_D = 200$ mV.

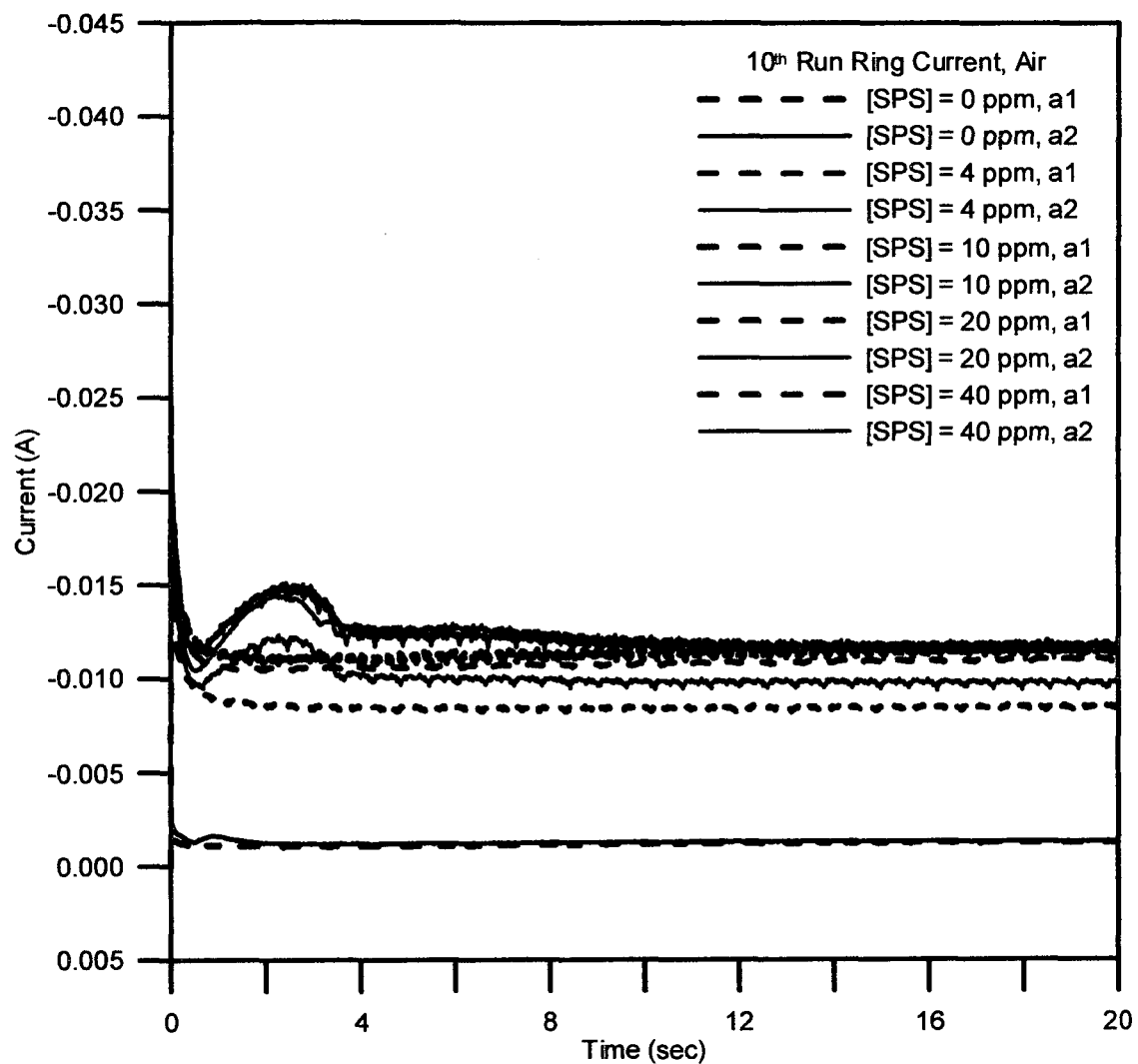


Figure 4.3 Ring current transients of 10th run without (dash line) and with (solid line) Cu (I) generation at the disk under air. [SPS] varies from 0 to 20 ppm. $\omega = 100$ rpm, $\Phi_D = 200$ mV.

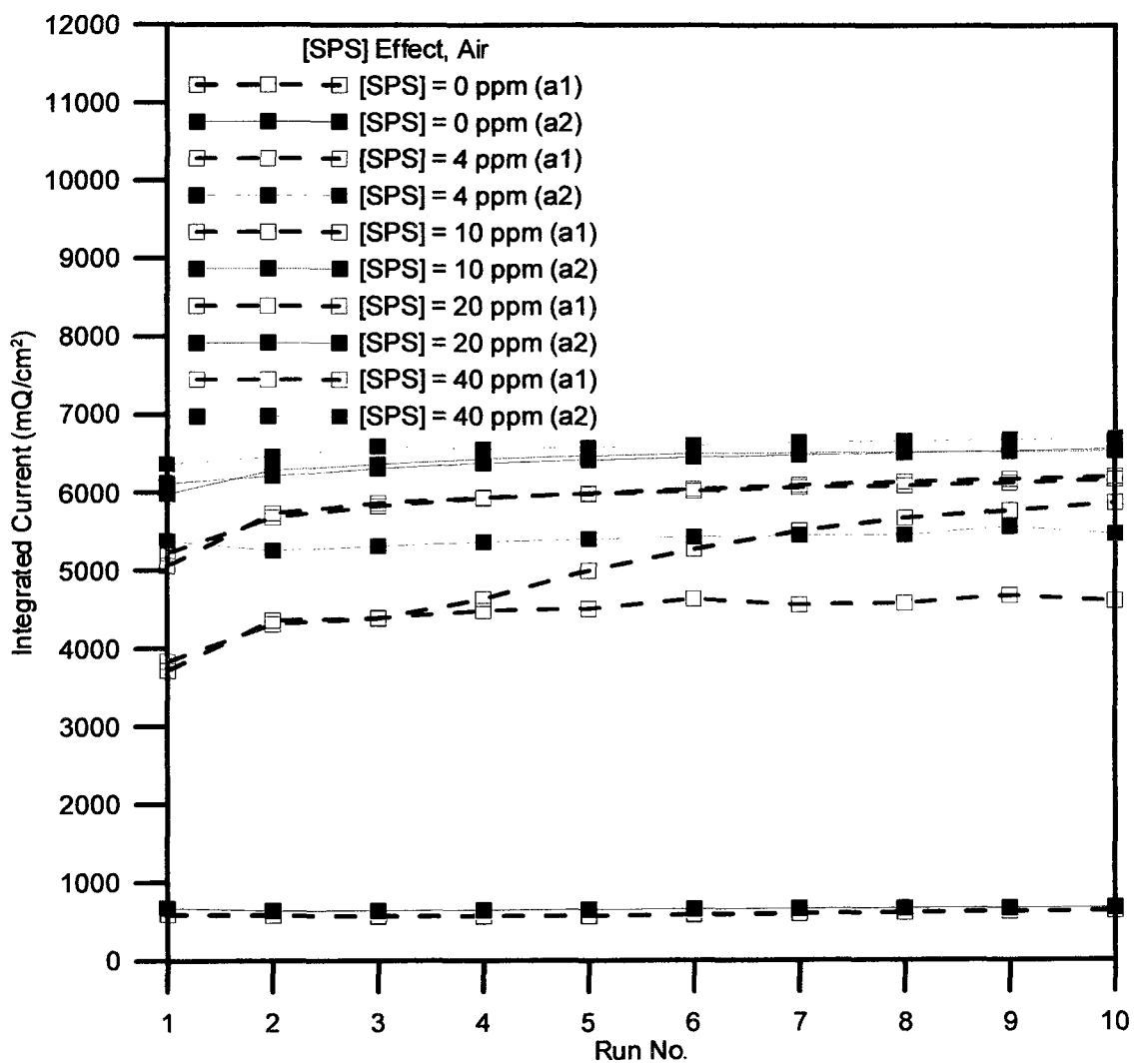


Figure 4.4 Successive ring integrated currents without and with Cu (I) production at the disk. Experiments are performed under air. [PEG] = 400 ppm, $\omega = 100$ rpm, $\Phi_D = 200$ mV.

4.1.2 Ring current transients under oxygen and argon

The experiments were run under oxygen or argon atmosphere to provide insight into the role of Cu (I). Because oxygen reacts with Cu (I) and oxidizes it into Cu (II), less Cu (I) is expected to be present in the solution under oxygen, resulting in reduced accelerant generation. In contrast, under argon the higher Cu (I) concentration should generate more accelerant.

In Figure 4.5, the ring charges without and with Cu (I) generation from the disk are shown under oxygen and argon respectively. Similar to the results with air saturated solution, there is no increase of charge from a1 to a2 in the absence of SPS. The maximum increase of charge on each corresponding run appears with an SPS concentration of 4 ppm. With higher SPS concentration up to 40 ppm, less increase of acceleration is observed. The steady state charges in the presence of higher SPS concentration for the last several runs with argon purging are higher than with oxygen purging. It is estimated that Cu (I) might be the limiting agent in the presence of higher SPS concentration and results in less acceleration.

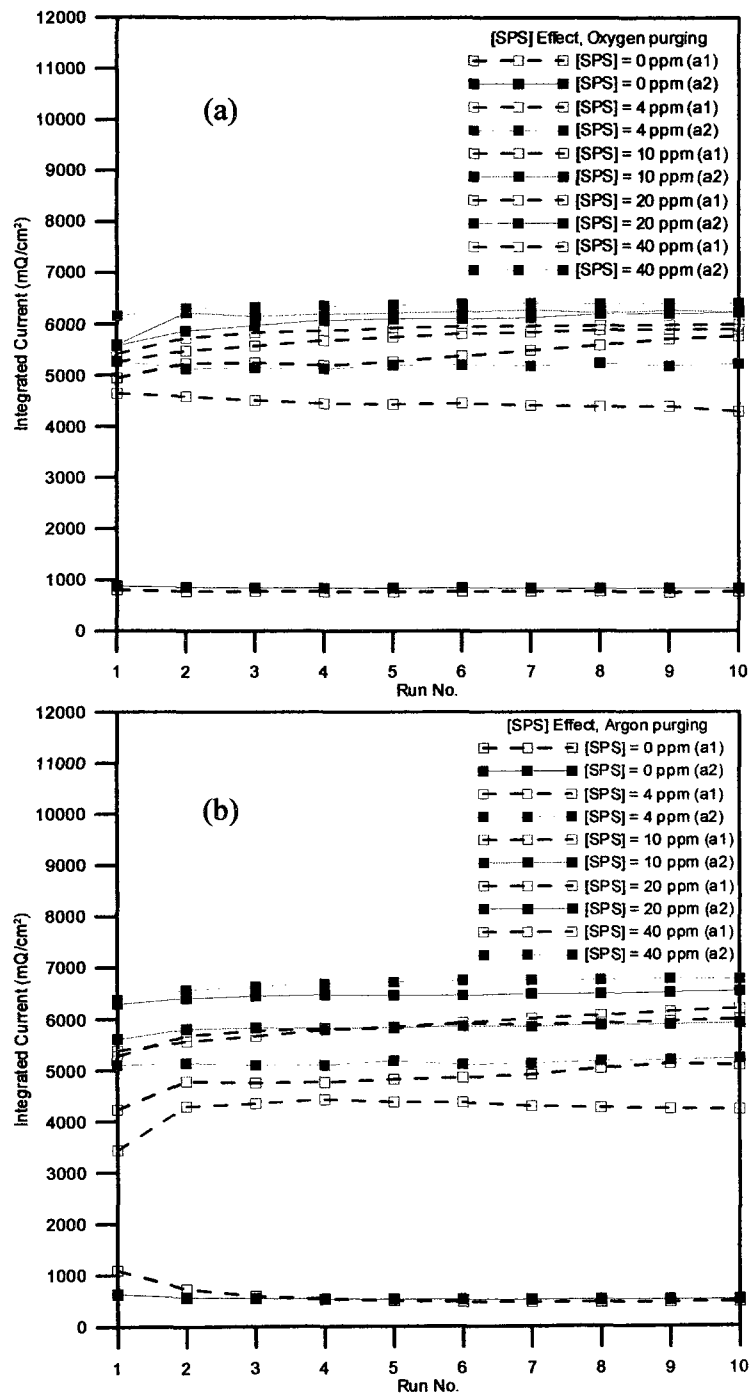


Figure 4.5 Successive ring integrated currents without and with Cu (I) production at the disk under (a) oxygen, and (b) argon. [PEG] = 400 ppm, $\omega = 100$ rpm, $\Phi_D = 200$ mV.

4.1.3 Cu (I) generation at the disk under air, oxygen, and argon

The integrated current results of procedure b1 and b2 are calculated based on (3.4) to obtain the ratio of partial current for Cu (I) generation at the disk to the total current shown (see Table 4.2). Both the ratio of Cu (I) partial current to total current and the total charge of Cu (I) generation are shown. Also, the average partial Cu (I) current from the disk as a function of SPS concentration under different gases is shown in Figure 4.6. When the solution is air saturated, the fractional Cu (I) partial current increases with consecutive runs and reaches a saturated level of about 18%. When the SPS concentration is lower, the acceleration produces less copper deposition, and more runs are required to bring Cu (I) to a saturated level. When SPS is added up to 40 ppm, the Cu (I) partial current increases to nearly the saturated level at run 2. This is consistent with the observations in Figure 4.4 that the saturated Cu (I) level limits the acceleration effect even if more SPS is present at concentration generation greater than 4 ppm. Under argon the saturated fractional Cu (I) partial current is nearly 20%, which is about 2% higher than under air. The fractional Cu (I) partial current under oxygen is about 14%, which is about 4% lower than under air.

Table 4.3 and Figure 4.7 show the average ring charge for the last 5 runs as a function of average Cu (I) stripping charge from the disk versus SPS concentrations. For all three gases, Cu (I) always increases with higher SPS concentration but reaches a saturated level so that the acceleration cannot promote more ring charge. Therefore, the ring charge values under different atmospheres are close at high SPS concentration (see Figure 4.7a). Figure 4.7b shows the increased percentage of ring charge from a1 to a2 presents largest increment in the presence of 4 ppm SPS, and then decreases with more SPS added. For oxygen, the increment of ring charge from a1 to a2 is lower, which fits

the model of consumption of Cu (I) by oxygen.

Table 4.2 Ratio of Cu (I) partial current to total disk current at successive runs under various SPS concentrations

Gas	[SPS]	Cu (I) partial current in each run									
		1	2	3	4	5	6	7	8	9	10
Air	0 ppm	12.2%	11.1%	11.0%	8.8%	10.7%	10.5%	10.5%	11.2%	10.7%	10.5%
	4 ppm	7.8%	8.5%	11.3%	12.9%	14.7%	16.1%	18.4%	17.3%	18.2%	17.7%
	10 ppm	10.8%	11.1%	13.3%	17.2%	17.5%	17.7%	17.9%	17.4%	17.0%	16.1%
	20 ppm	11.5%	17.9%	17.3%	16.9%	16.9%	17.1%	17.4%	17.5%	17.6%	17.9%
	40 ppm	15.5%	17.4%	17.8%	17.7%	17.7%	17.7%	17.7%	17.6%	17.6%	17.8%
O ₂	0 ppm	10.8%	11.1%	10.6%	9.9%	9.8%	9.6%	9.8%	10.4%	10.8%	9.8%
	4 ppm	11.3%	12.2%	13.4%	14.0%	14.8%	16.0%	16.6%	16.4%	16.6%	17.7%
	10 ppm	6.8%	8.4%	9.1%	10.5%	12.5%	13.7%	15.6%	15.9%	15.9%	16.0%
	20 ppm	11.6%	12.6%	13.2%	14.0%	14.3%	14.0%	14.1%	14.1%	14.1%	14.0%
	40 ppm	10.6%	14.1%	14.0%	14.6%	14.9%	15.0%	14.8%	14.7%	16.4%	14.0%
Ar	0 ppm	11.7%	12.7%	10.8%	11.5%	8.0%	11.4%	10.6%	10.4%	9.5%	10.0%
	4 ppm	11.0%	9.9%	11.7%	12.8%	14.0%	15.4%	15.8%	18.5%	18.4%	18.4%
	10 ppm	11.3%	10.5%	11.4%	14.6%	16.0%	17.4%	18.4%	18.6%	19.1%	19.0%
	20 ppm	13.6%	12.5%	14.1%	17.3%	19.0%	19.7%	20.3%	20.6%	20.3%	20.9%
	40 ppm	14.0%	13.2%	14.4%	16.6%	18.5%	18.9%	19.5%	19.7%	19.4%	19.7%

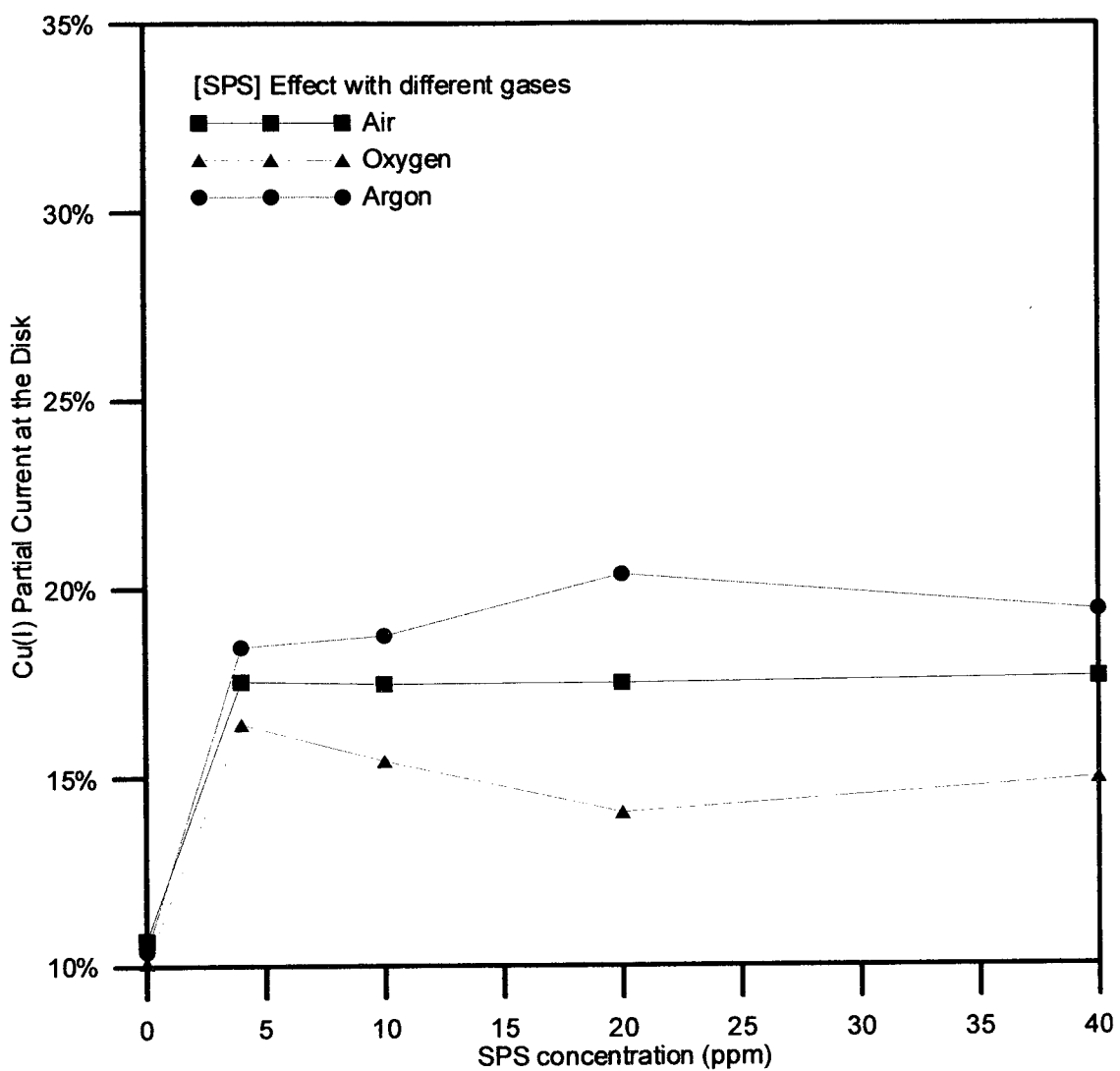


Figure 4.6 Cu(I) partial current at disk as a function of SPS concentration under different gases.

Table 4.3 Average Cu (I) partial current from disk and ring charge with Cu (I) generation (procedure a2) under various SPS concentrations

Gas	[SPS]	Average Cu (I)	Average Ring Charge at	Increased Percentage
		Partial Current	Procedure a2 (mQ/cm ²)	from a1 to a2
Air	0 ppm	10.7%	669	9.1%
	4 ppm	17.5%	5484	18.6%
	10 ppm	17.5%	6527	16.2%
	20 ppm	17.5%	6506	7.0%
	40 ppm	17.6%	6669	8.2%
O ₂	0 ppm	10.1%	840	8.7%
	4 ppm	16.4%	5217	17.9%
	10 ppm	15.4%	6260	11.9%
	20 ppm	14.1%	6170	5.2%
	40 ppm	15.0%	6414	7.2%
Ar	0 ppm	10.4%	522	9.2%
	4 ppm	18.5%	5175	20.8%
	10 ppm	18.8%	5881	17.5%
	20 ppm	20.4%	6492	9.6%
	40 ppm	19.4%	6773	11.6%

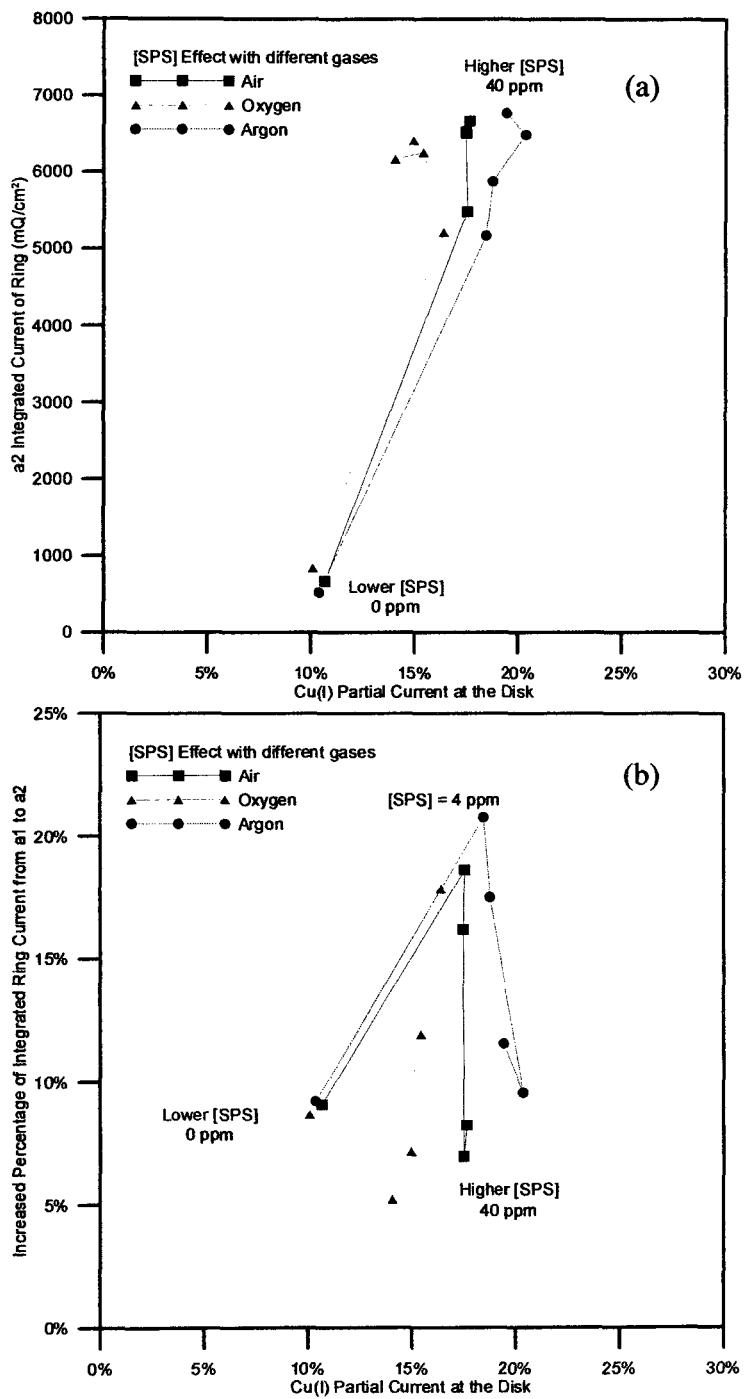


Figure 4.7 (a) Average ring charge with Cu (I) generation, and (b) Increased percentage of ring charge from a1 to a2 as a function of Cu (I) partial current at disk by SPS concentration variation under air, oxygen, and argon.

4.2 Effect of rotation speed

The RRDE rotation speed was varied from 5 to 400 rpm to observe how the interaction between Cu (I) and SPS is affected by different convective diffusion rates. The experiment was performed under three atmospheres: air, oxygen, and argon.

4.2.1 Ring current transients under air – with and without additives

First, the plating bath with PEG, SPS, and Cl^- was tested. Figure 4.8 shows the ring current response without and with Cu (I) generation at the disk at 5 rpm. Cu (I) was stripped from the disk over a period of 4 seconds, and the ring current increased during the same period. Results for a rotation speed of 400 rpm are shown in Figure 4.9. The peak occurring around 1.8 sec results from the release of Cu (I) to produce the accelerant. A current increment from a1 to a2 is observed. In Figure 4.10, the ring current of the 10th run at a given rotation speed without and with Cu (I) generated at the disk is shown under varying rotation speed. The temporary acceleration is highly dependent on the convective diffusion speed, and the acceleration is enhanced in shorter time with higher rotation speed. In Figure 4.11a, a charge increase from a1 to a2 is observed with $\omega \geq 25$ rpm, and this increase is slightly enlarged with higher rotation speed. On the other hand, there was little current increase at lower rotation speeds. Evidently, the accelerant is not produced without effective transport of Cu (I) from the disk to the ring. The plating bath including only copper sulfate, sulfuric acid, and chloride (Figure 4.11b) shows limited charge increase from a1 to a2. A comparison of the ring current density difference from a1 to a2 in Figure 4.12 even shows about 70 mA/cm² if there is no PEG/SPS in the plating electrolyte. The current difference from a1 to a2 is basically independent of rotation

speed in the absence of PEG and SPS.

4.2.2 Ring current transients under oxygen and argon

Figure 4.13 shows the integrated ring current without and with Cu (I) generation under oxygen. Similar to the previous result with air, the integrated ring current at lower rotation speed slightly increases, and starts to enlarge with runs and higher rotation speed from procedure a1 to a2.

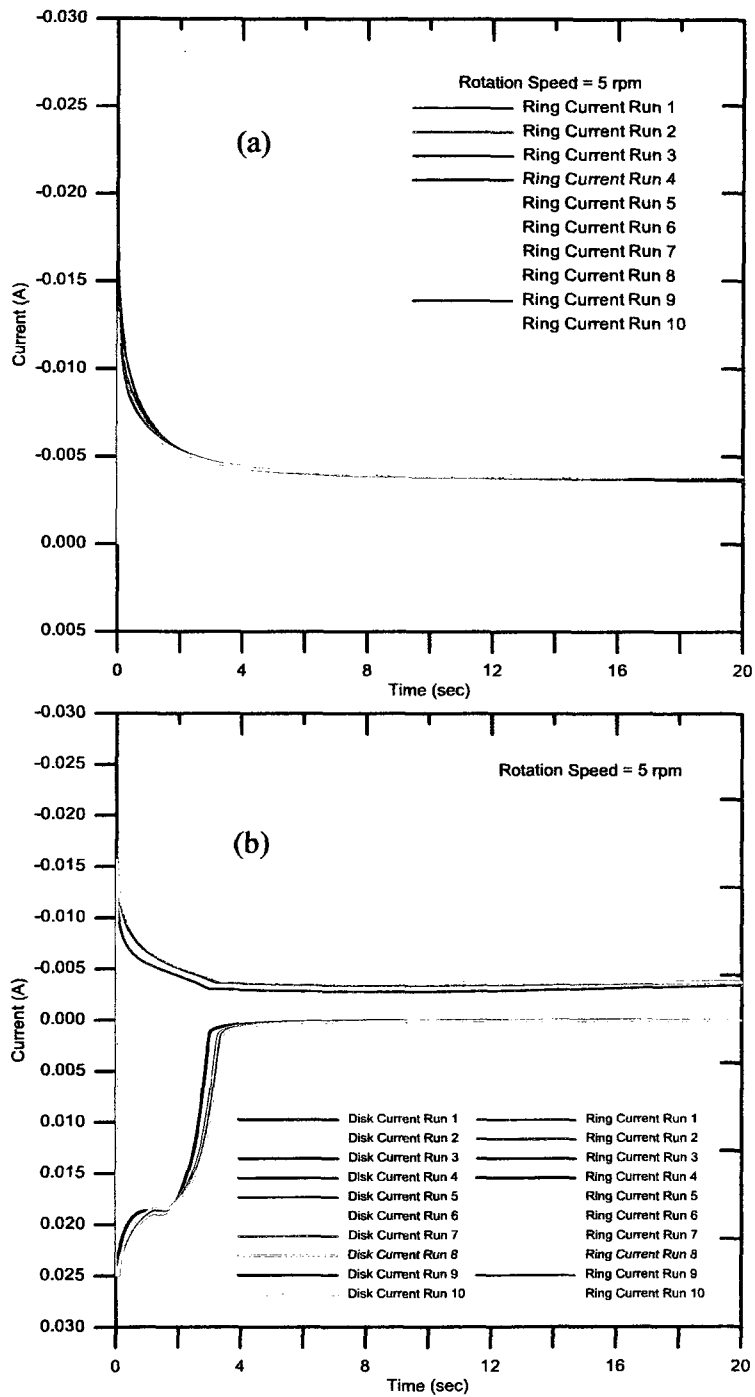


Figure 4.8 Ring current transients under air; (a) without Cu (I) generation at the disk; (b): with Cu (I) generation at the disk. [PEG] = 400 ppm, [SPS] = 10 ppm, $\omega = 5$ rpm, $\Phi_D = 200$ mV.

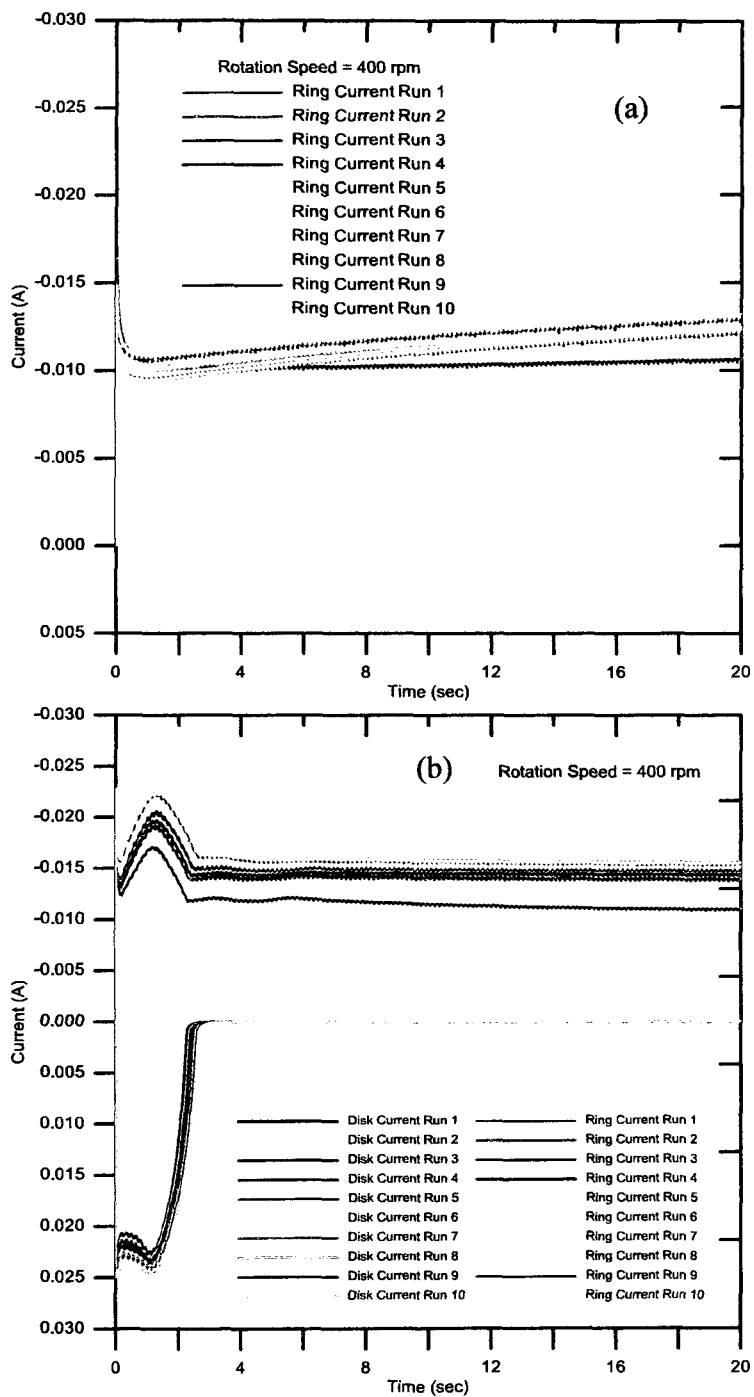


Figure 4.9 Ring current transients under air; (a) without Cu (I) generation at the disk; (b) with Cu (I) generation at the disk. [PEG] = 400 ppm, [SPS] = 10 ppm, $\omega = 400$ rpm, $\Phi_D = 200$ mV.

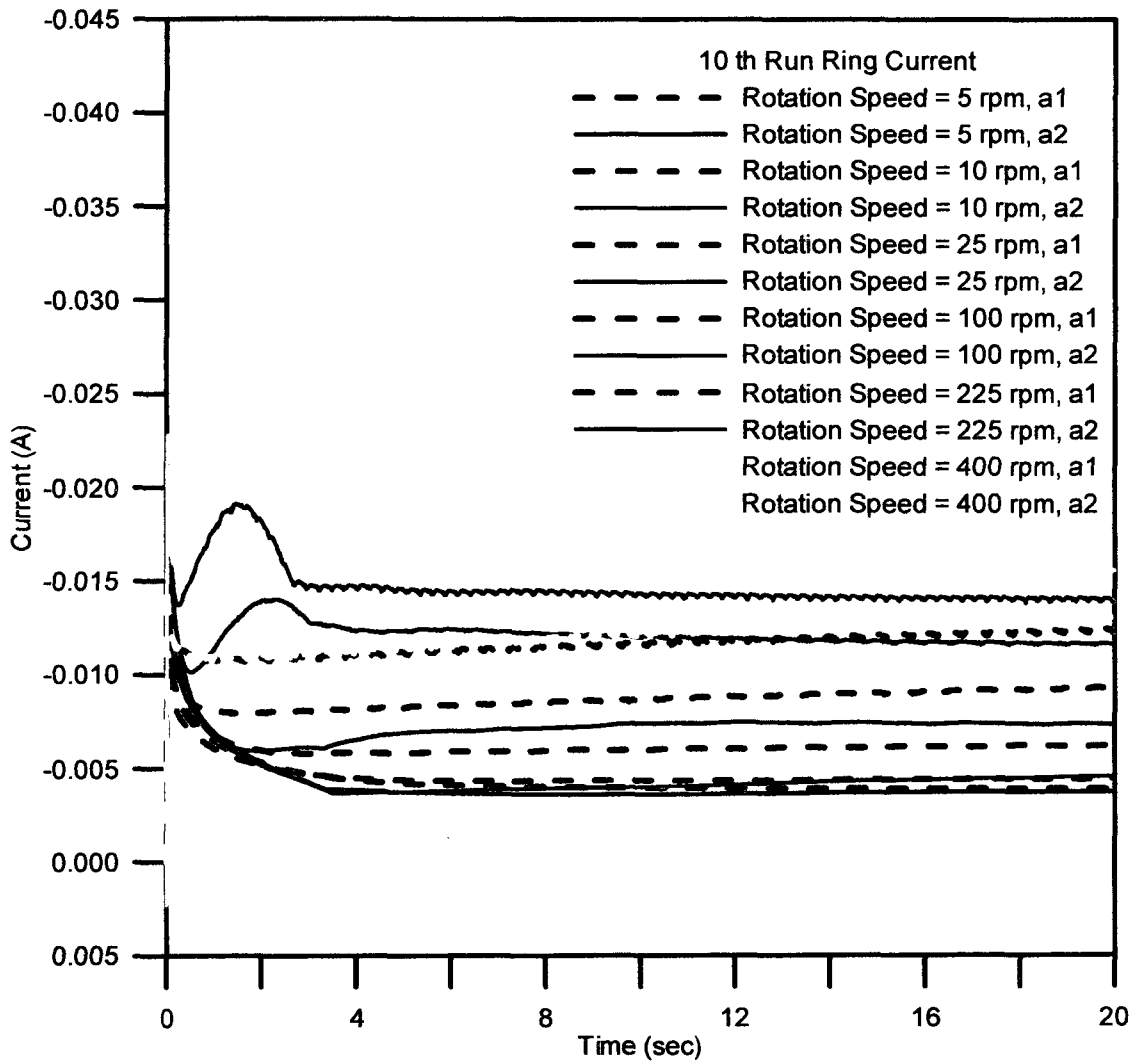


Figure 4.10 Ring current transients of 10th run without (dash line) and with (solid line) Cu (I) generation at the disk under air. [SPS] = 10 ppm, ω varies from 5 to 400 rpm, $\Phi_D = 200$ mV.

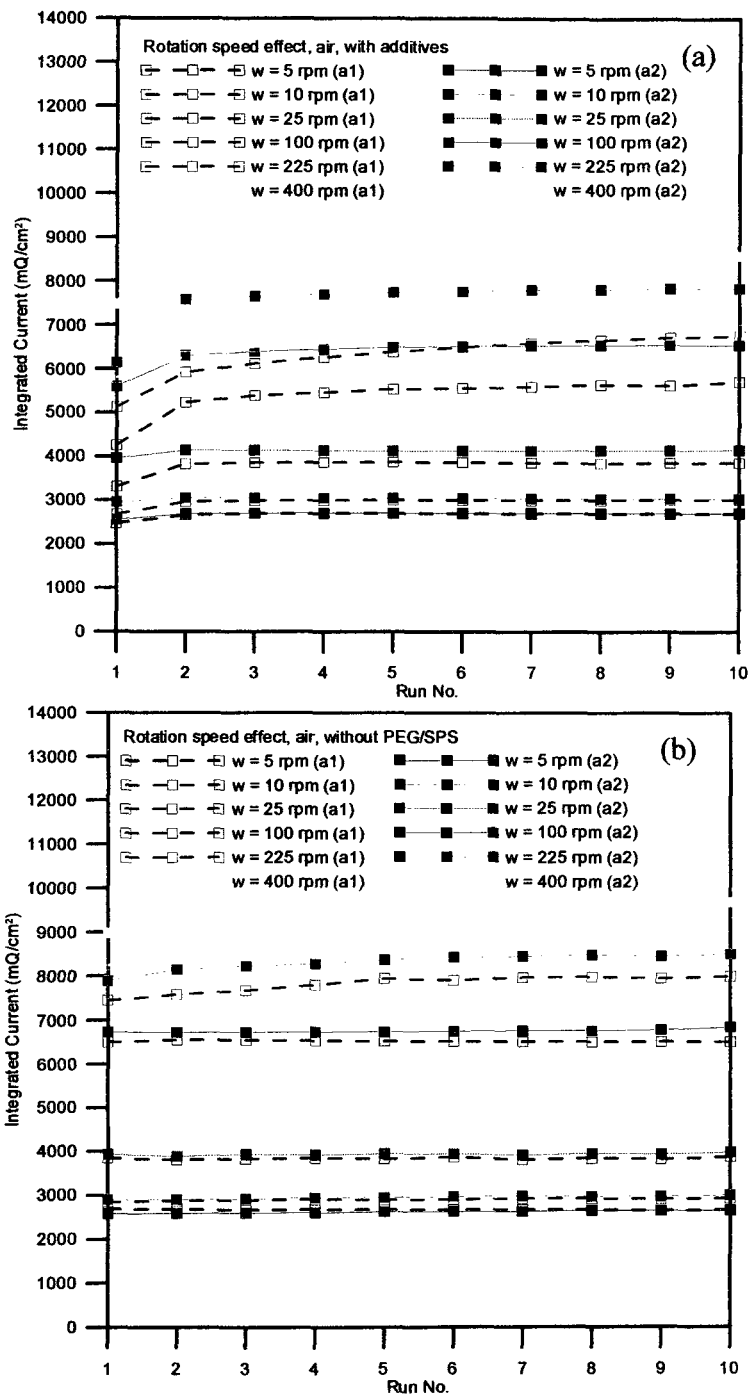


Figure 4.11 Successive ring integrated current without and with Cu (I) production at the disk. Experiments are performed under air. $\omega = 100$ rpm, $\Phi_D = 200$ mV. (a) with additives; (b) without PEG/SPS.

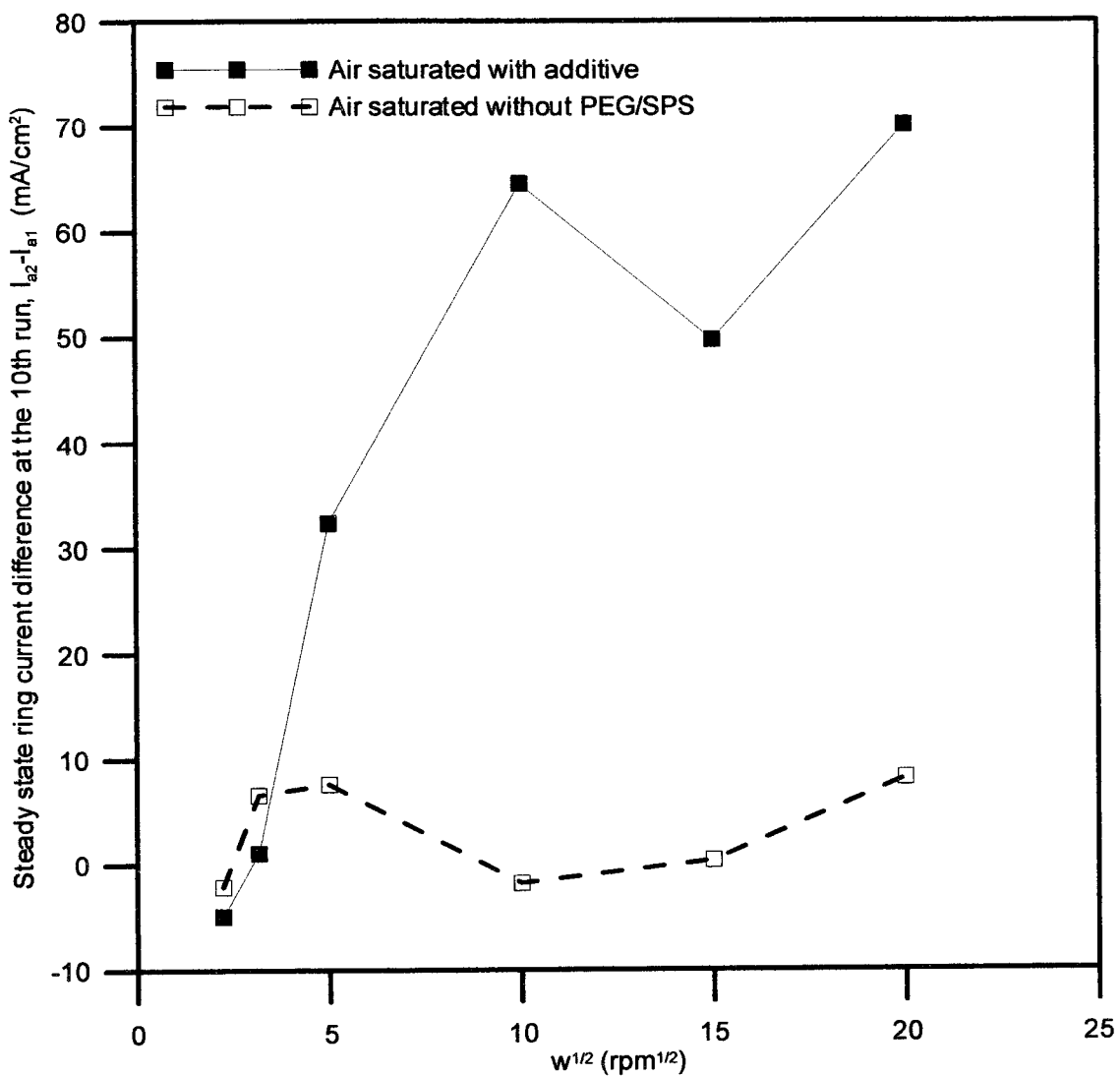


Figure 4.12 The rotation speed effect of steady ring current density difference of the 10th run from a1 to a2. Solid line: PEG = 400 ppm, SPS = 10 ppm; dash line: PEG = 0 ppm, SPS = 0 ppm.

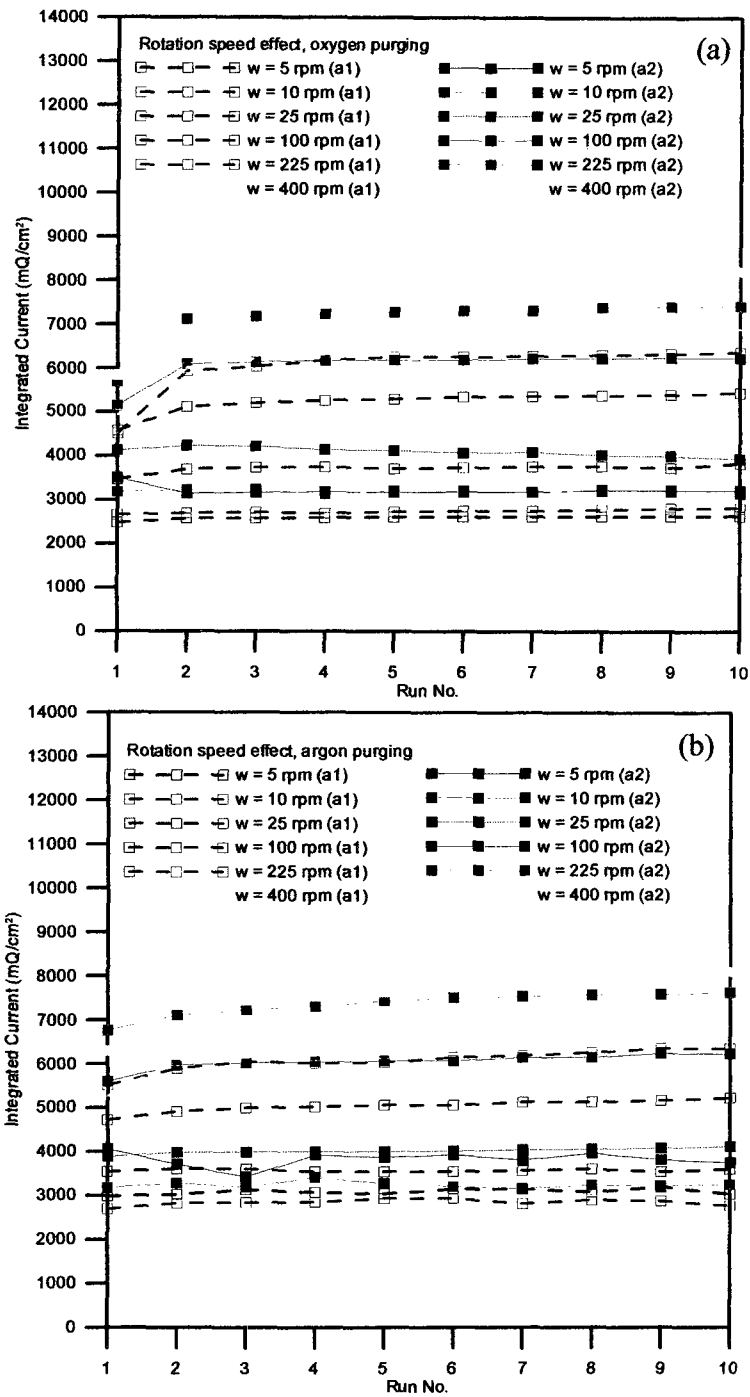


Figure 4.13 Successive ring integrated current without and with Cu (I) production at the disk. Experiments are performed under (a) oxygen, and (b) argon. [PEG] = 400 ppm, [SPS] = 10 ppm, $\Phi_D = 200$ mV.

4.2.3 Cu (I) generation at the disk under air, oxygen, and argon

The ratio of Cu (I) partial current to total disk-stripping current is shown in Table 4.4 and Figure 4.14. For the solution without additives and under the air, Cu (I) partial current is much lower. When additives are added into the solution, the Cu (I) partial current is 10 times larger and it is dependent on rotation speed.

The Cu (I) partial current is 1~6% lower under oxygen while it is 2~4% higher under argon compared to the condition under air. In Table 4.5 and Figure 4.15, the average ring charge for the last 5 runs are plotted against the Cu (I) disk stripping charge at several rotation speeds. The ring charge increases with increasing rotation speed under three gases, but it is found that the ring charge under argon is less than the other conditions (see Figure 4.15a).

Table 4.4 Ratio of Cu (I) partial current to total disk current at successive runs under rotation speed variation

Gas	Rotation	Cu (I) partial current in each run									
	Speed	1	2	3	4	5	6	7	8	9	10
Air No Add	5 rpm	0.5%	0.5%	0.5%	0.7%	0.6%	0.6%	0.6%	0.7%	0.3%	0.8%
	10 rpm	0.5%	0.6%	0.5%	0.5%	0.5%	0.5%	0.6%	0.5%	0.5%	0.6%
	25 rpm	0.4%	0.6%	0.3%	0.6%	0.5%	0.4%	0.7%	0.4%	0.4%	0.4%
	100 rpm	1.1%	0.8%	0.5%	0.8%	1.1%	0.7%	1.0%	0.4%	1.5%	0.8%
	225 rpm	1.5%	1.5%	1.5%	1.6%	1.7%	1.5%	1.5%	2.0%	1.4%	1.5%
	400 rpm	2.2%	2.5%	2.5%	2.4%	2.6%	2.5%	2.6%	2.6%	2.8%	2.7%
Air	5 rpm	3.2%	7.1%	7.8%	7.9%	8.1%	7.8%	8.2%	8.1%	8.3%	7.8%
	10 rpm	5.5%	5.9%	6.8%	8.1%	8.6%	8.3%	8.6%	9.0%	8.8%	8.8%
	25 rpm	5.5%	7.4%	8.9%	9.3%	9.5%	10.0%	9.9%	9.2%	9.1%	9.8%
	100 rpm	10.8%	11.1%	13.3%	17.2%	17.5%	17.7%	17.9%	17.4%	17.0%	16.1%
	225 rpm	15.0%	18.5%	25.3%	25.7%	26.2%	25.8%	25.7%	25.8%	25.3%	25.1%
	400 rpm	19.2%	21.1%	27.8%	31.6%	31.8%	32.7%	29.5%	33.0%	34.3%	33.9%
O ₂	5 rpm	5.2%	5.9%	6.9%	6.9%	6.6%	6.4%	6.8%	6.8%	6.0%	6.7%
	10 rpm	3.9%	5.5%	6.0%	6.2%	7.0%	7.1%	6.9%	7.1%	10.2%	6.3%
	25 rpm	5.4%	6.4%	6.7%	6.9%	8.4%	8.0%	8.0%	8.1%	9.1%	8.1%
	100 rpm	6.8%	8.0%	8.7%	10.1%	12.1%	13.3%	15.3%	15.6%	15.6%	16.4%
	225 rpm	11.8%	12.4%	14.6%	16.5%	18.0%	21.0%	25.3%	23.5%	20.5%	20.4%
	400 rpm	16.9%	17.1%	19.7%	23.2%	25.6%	26.9%	26.9%	27.1%	27.0%	26.5%
Ar	5 rpm	7.2%	7.0%	7.2%	8.0%	8.6%	9.4%	9.7%	11.0%	11.3%	11.6%
	10 rpm	8.8%	6.6%	7.7%	9.9%	9.3%	10.6%	14.1%	11.6%	11.3%	12.1%
	25 rpm	8.9%	8.3%	9.8%	12.6%	12.3%	14.6%	14.8%	14.9%	14.5%	14.7%
	100 rpm	11.3%	10.5%	11.4%	14.6%	16.0%	17.4%	18.4%	18.6%	19.1%	19.0%
	225 rpm	19.0%	17.7%	18.3%	22.2%	24.6%	26.1%	27.1%	28.0%	27.9%	27.8%
	400 rpm	23.0%	22.9%	25.4%	34.7%	33.2%	33.6%	34.0%	34.1%	34.1%	32.6%

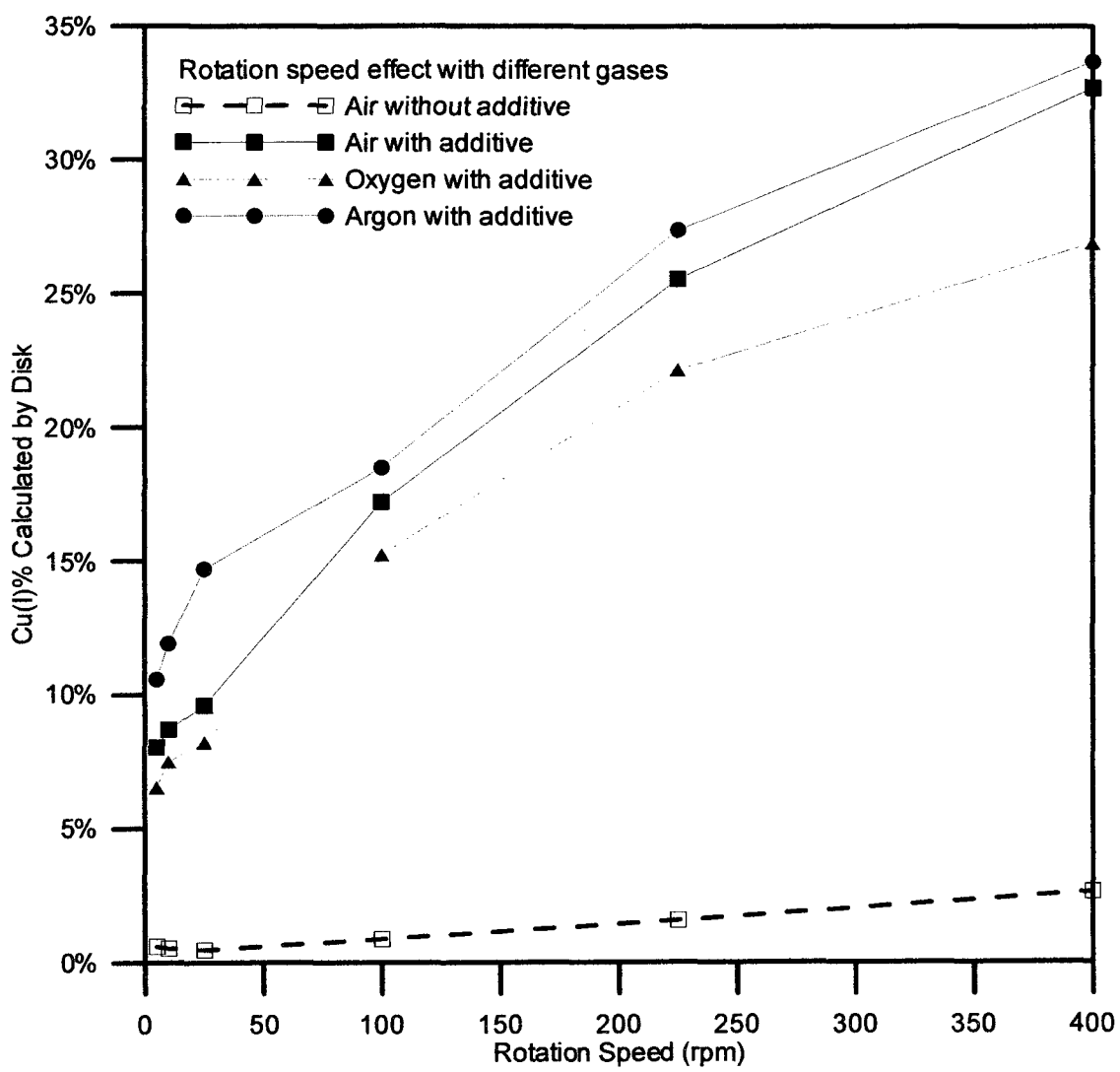


Figure 4.14 Average Cu (I) partial current at the disk as a function of rotation speed under various gases.

Table 4.5 Average Cu (I) partial current ratio from disk and ring charge with Cu (I) generation (procedure a2)

Gas	Rotation Speed	Average Cu (I)	Average Ring Charge	Increased Percentage from a1 to a2
		Partial Current Ratio	at Procedure a2 (mQ/cm ²)	
Air No Add	5 rpm	0.6%	2639	-0.9
	10 rpm	0.5%	2984	2.1
	25 rpm	0.5%	3944	2.6
	100 rpm	0.9%	6779	4.1
	225 rpm	1.6%	8465	6.3
	400 rpm	2.6%	9623	8.8
Air	5 rpm	8.0%	2709	0.4
	10 rpm	8.7%	3046	1.1
	25 rpm	9.6%	4146	7.3
	100 rpm	17.2%	6543	16.2
	225 rpm	25.5%	7819	17.5
	400 rpm	32.7%	8548	21.8
O ₂	5 rpm	6.5%	3212	22.1
	10 rpm	7.5%	3196	14.5
	25 rpm	8.2%	4032	6.8
	100 rpm	15.2%	6231	15.5
	225 rpm	22.2%	7376	16.7
	400 rpm	26.9%	8183	20.9
Ar	5 rpm	10.6%	3853	23.5
	10 rpm	11.9%	3220	12.5
	25 rpm	14.7%	4064	13.6
	100 rpm	18.5%	6158	19.9
	225 rpm	27.4%	7569	20.8
	400 rpm	33.7%	7937	22.6

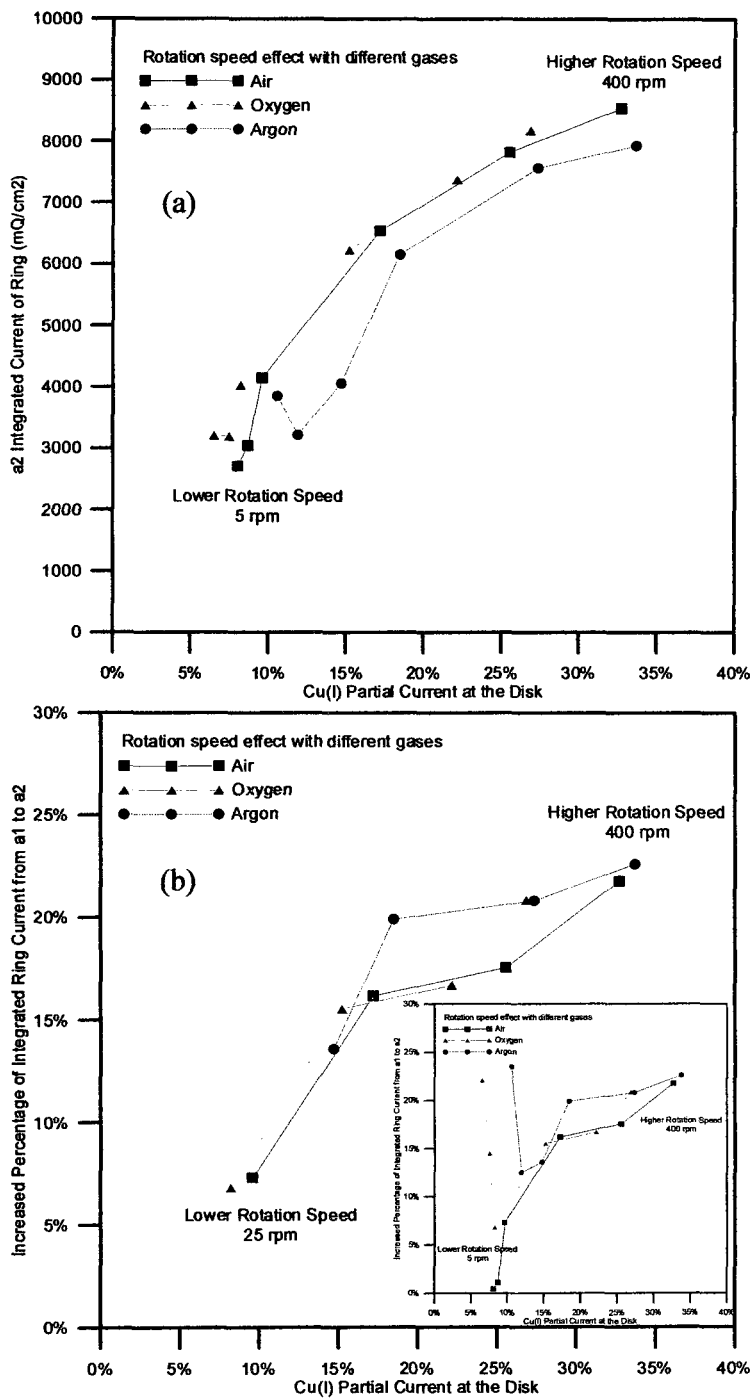


Figure 4.15 (a) Average ring charge with Cu (I) generation, and (b) Increased percentage of ring charge from a1 to a2 as a function of Cu (I) partial current at disk by rotation speed variation under air, oxygen, and argon.

4.3 Effect of disk stripping potential

The disk-stripping potential should have a strong influence on the generation of Cu (I). The Cu (0) / Cu (I) couple has fast kinetics and can be assumed to be at interfacial equilibrium. According to the Nernst equation, the equilibrium concentration rises exponentially with increasing positive potential. At the same time, the kinetically limited conversion of Cu (I) to Cu (II) increases with increasing positive potential. Hence we expect interfacial Cu (I) concentration and Cu (I) flux from the disk to rise with increasing potential, pull through a maximum and then fall.

4.3.1 Ring current transients with air saturated – with and without additives

Figure 4.16 shows the ring current response without and with Cu (I) stripping at 100 mV with SPS and PEG present in the solution. The ring current is found to increase from a1 to a2. In Figure 4.17, the ring currents of the 10th runs without and with Cu (I) generation at the disk are shown for various stripping potentials. The temporary acceleration is dependent on the disk stripping potential. When the stripping potential is small (100 mV), it takes longer to release cuprous ions and hence the temporary acceleration duration lasts up to 14 seconds. When the stripping potential is increased above 150 mV, the copper is stripped in a shorter time and the accelerant causes an abrupt ring-current increase. The ring charge without and with Cu (I) generation at the disk is shown Figure 4.18a. The charge increased from a1 to a2. However, the increment from a1 to a2 is independent of stripping potential. Figure 4.18b shows the integrated ring current without and with Cu (I) generation from the disk without PEG and SPS. The ring charge slightly increases from a1 to a2, but it is still independent of stripping potential.

4.3.2 Ring current transients under oxygen and argon

Figure 4.19 shows the ring charges without and with Cu (I) generation from the disk under oxygen or argon.

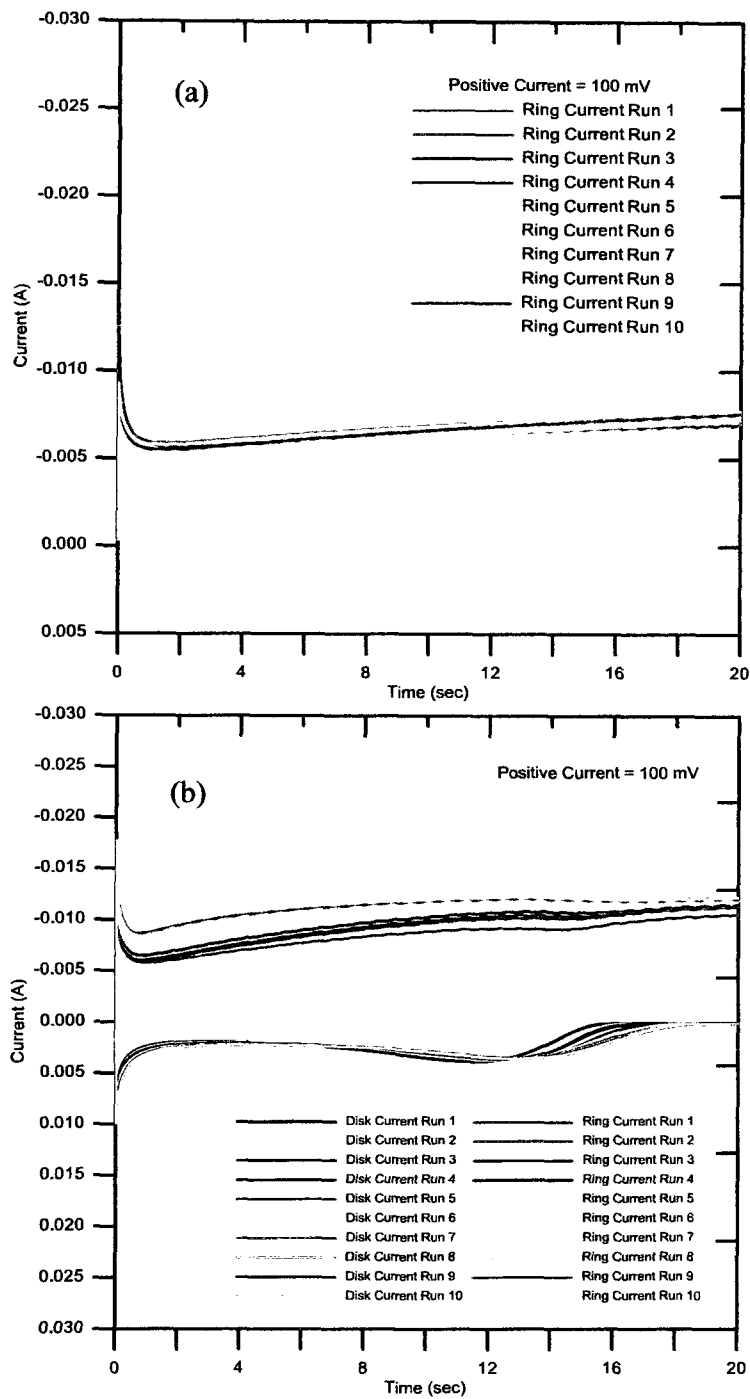


Figure 4.16 Ring current transients under air; top: without Cu (I) generation at the disk; bottom: with Cu (I) generation at the disk. [PEG] = 400 ppm, [SPS] = 10 ppm, $\omega = 100$ rpm, $\Phi_D = 100$ mV.

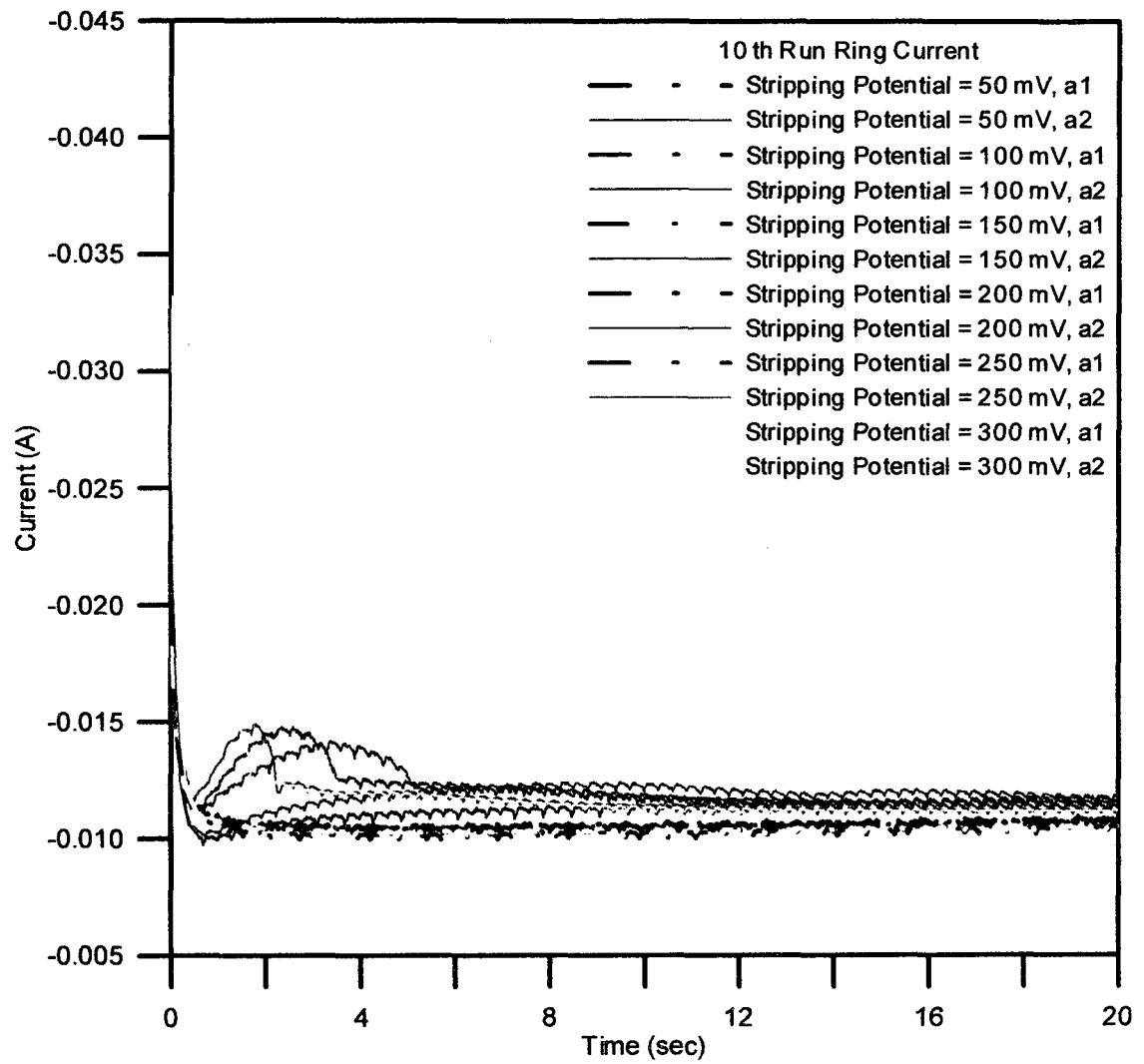


Figure 4.17 Ring current transients of 10th run without (dash line) and with (solid line) Cu (I) generation at the disk under air. [SPS] = 10 ppm, $\omega = 100$ rpm, Φ_D varies from 100 to 200 mV.

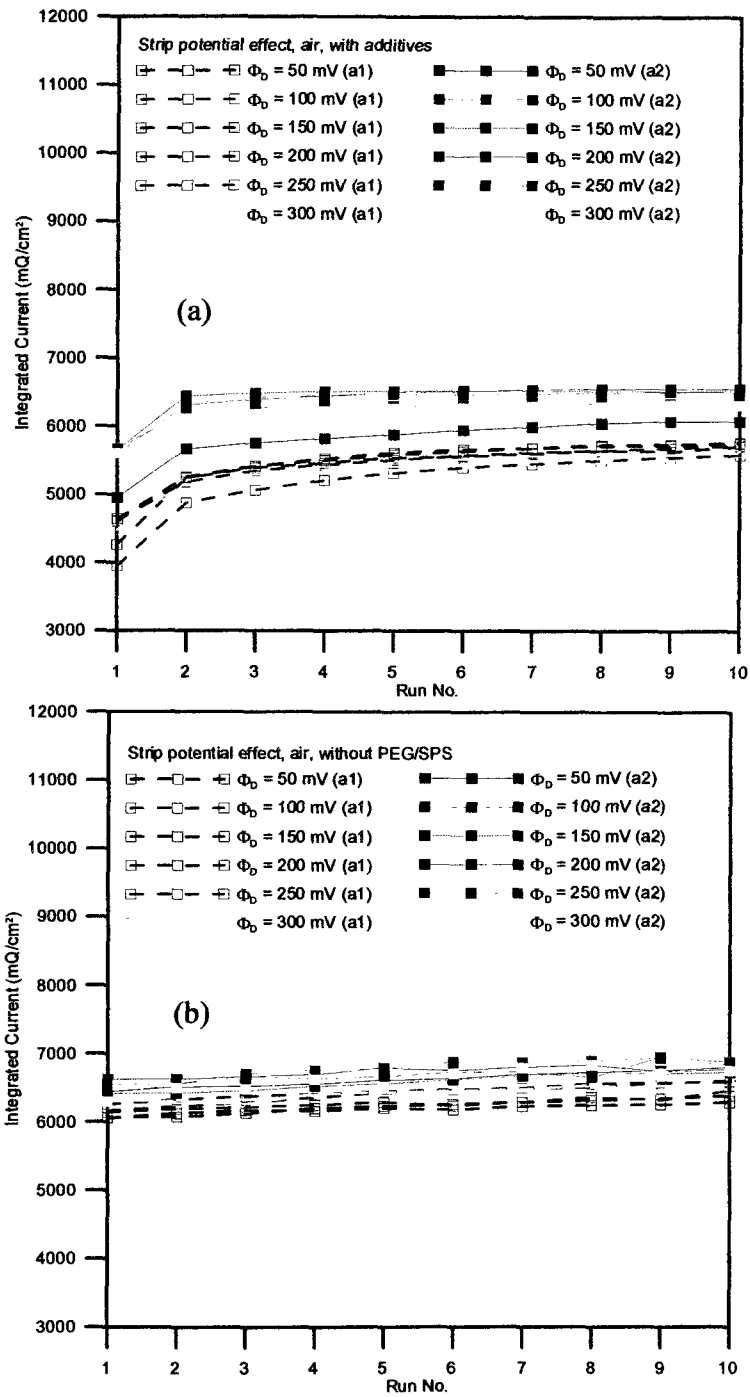


Figure 4.18 Successive ring integrated current without and with Cu (I) production at the disk. Experiments are performed under air. SPS = 100 ppm, $\omega = 100$ rpm. (a) with additives; (b) without PEG/SPS.

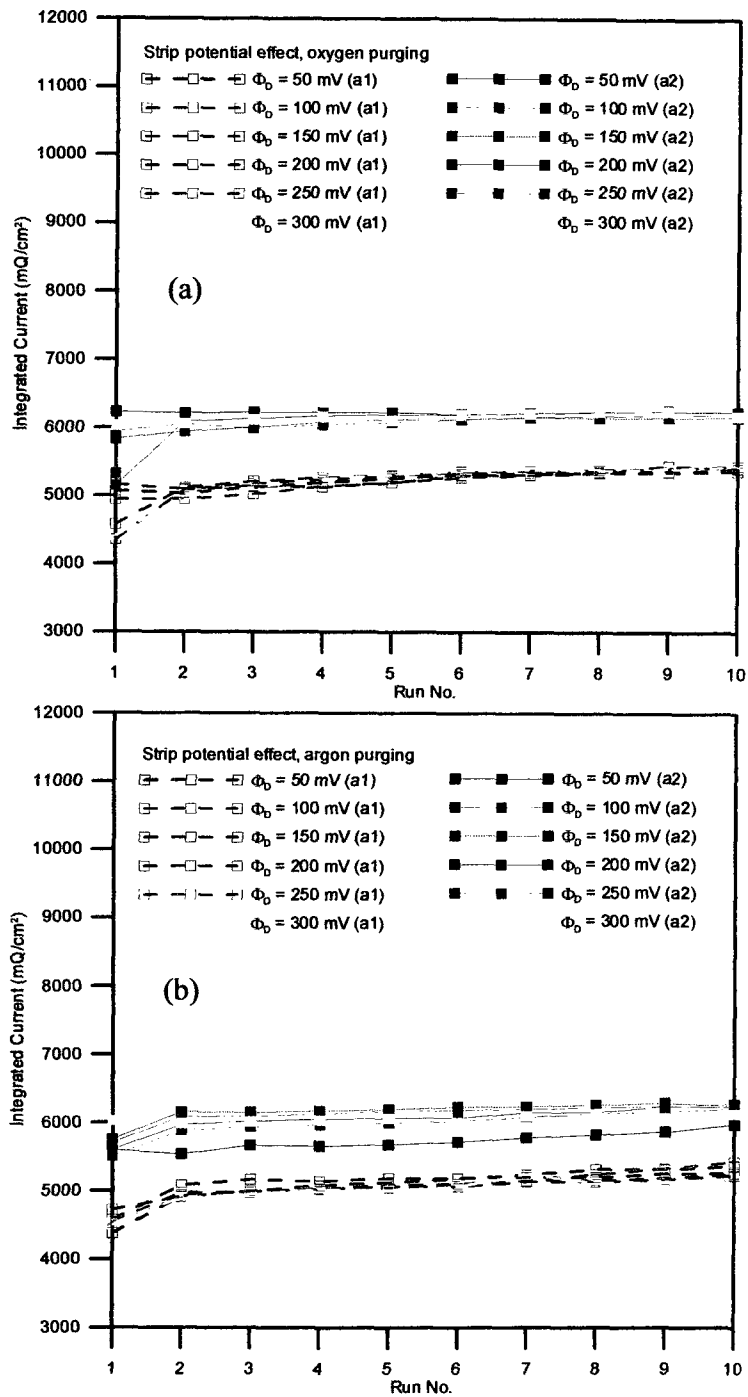


Figure 4.19 Successive ring integrated current without and with Cu (I) production at the disk. Experiments are performed under (a) oxygen; (b) argon. [PEG] = 400 ppm, [SPS] = 10 ppm, $\omega = 100$ rpm.

4.3.3 Cu (I) generation at the disk under air, oxygen, and argon

The Cu (I) partial current is shown in Table 4.6 and Figure 4.20. A higher Cu (I) partial current is obtained when copper is oxidized at lower stripping potential. For the solution without additives under air, Cu (I) generation is still very low.

The overall comparison of stripping variation under oxygen, air and argon is shown in Table 4.7 and Figure 4.21. The Cu (I) partial current has a strong dependence on the disk stripping potential; however, the ring charge is independent of stripping potential. The increment of ring charge from a1 to a2 in Figure 4.21b shows the largest increase under argon, and the increments of ring charge under air and oxygen are about the same.

Table 4.6 Ratio of Cu (I) partial current to total disk current at successive runs under stripping potential variation

Gas	Strip	Cu (I) % in each run									
	Potential	1	2	3	4	5	6	7	8	9	10
	100 mV	1.2%	1.1%	1.3%	1.4%	1.3%	1.2%	1.3%	1.2%	1.5%	1.4%
	150 mV	0.9%	0.9%	1.1%	1.1%	1.0%	1.3%	1.2%	1.0%	1.0%	1.1%
Air	200 mV	1.1%	0.8%	0.5%	0.8%	1.1%	0.7%	1.0%	0.4%	1.5%	0.8%
Add	250 mV	1.2%	0.7%	0.7%	0.8%	0.7%	0.5%	1.0%	0.8%	0.9%	0.8%
	300 mV	0.6%	1.0%	0.7%	0.9%	1.4%	1.0%	1.1%	0.9%	1.0%	1.1%
Air	100 mV	13.9%	15.7%	15.6%	15.8%	16.0%	15.5%	16.0%	15.5%	15.8%	15.8%
	150 mV	11.5%	13.3%	14.3%	14.5%	14.6%	14.7%	14.5%	15.0%	15.2%	15.1%
	200 mV	10.8%	11.1%	13.3%	17.2%	17.5%	17.7%	17.9%	17.4%	17.0%	16.1%
	250 mV	7.9%	6.8%	7.9%	8.8%	9.0%	9.1%	8.7%	8.3%	8.1%	8.2%
	300 mV	5.3%	5.3%	5.4%	6.1%	6.3%	6.0%	5.8%	6.2%	6.0%	5.7%
O ₂	100 mV	10.1%	12.7%	13.5%	13.1%	13.4%	13.6%	13.6%	13.7%	14.1%	14.5%
	150 mV	5.2%	8.8%	8.5%	7.7%	11.8%	11.4%	19.6%	13.4%	13.5%	13.0%
	200 mV	6.8%	8.0%	8.7%	10.1%	12.1%	13.3%	15.3%	15.6%	15.6%	16.4%
	250 mV	6.6%	7.0%	7.1%	7.9%	7.8%	7.9%	7.7%	7.9%	7.6%	7.8%
	300 mV	5.4%	4.9%	5.4%	5.2%	6.2%	4.9%	5.6%	5.4%	5.1%	5.6%
Ar	100 mV	13.5%	15.4%	16.2%	17.1%	17.2%	17.6%	17.1%	17.9%	17.6%	17.5%
	150 mV	15.4%	16.1%	16.6%	17.4%	17.6%	18.0%	17.5%	17.1%	17.3%	17.2%
	200 mV	11.3%	10.5%	11.4%	14.6%	16.0%	17.4%	18.4%	18.6%	19.1%	19.0%
	250 mV	7.9%	7.1%	8.3%	9.3%	9.8%	11.1%	12.4%	12.9%	12.7%	12.4%
	300 mV	5.0%	5.9%	5.2%	5.8%	6.6%	6.3%	6.9%	7.2%	7.0%	6.7%

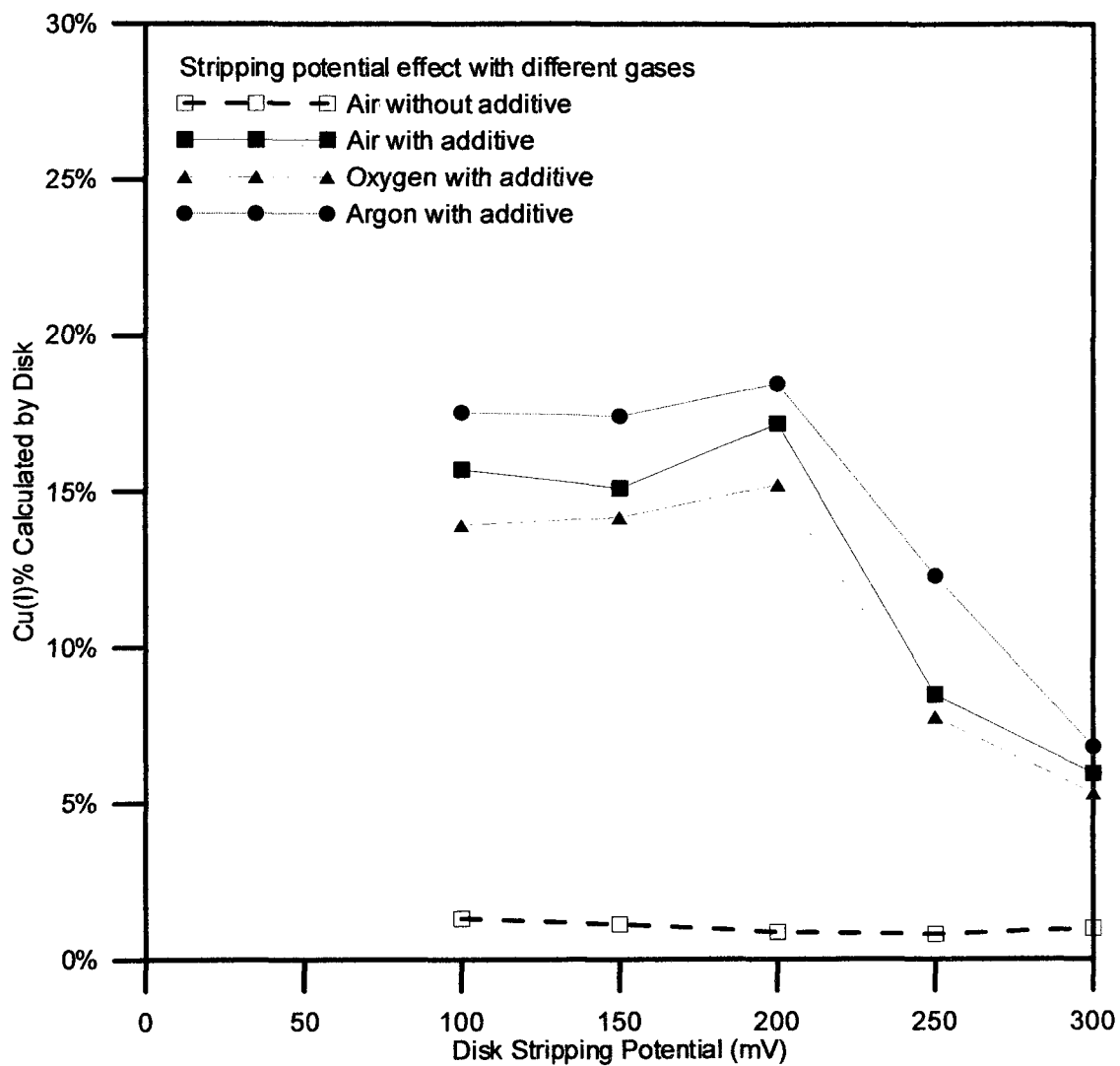


Figure 4.20 Cu (I) partial current at the disk as a function of stripping potential with various gases.

Table 4.7 Average Cu (I) partial current ratio from disk and ring charge with Cu (I) generation (procedure a2)

Gas	Strip Potential	Average Cu (I)	Average Ring Charge	Increased Percentage from a1 to a2
		Partial Current Ratio	at Procedure a2 (mQ/cm ²)	
Air	100 mV	2.0%	6720	6.4%
	150 mV	1.3%	6792	7.2%
	200 mV	1.1%	6690	7.2%
	250 mV	0.9%	6779	3.8%
	300 mV	0.8%	6884	5.3%
Air	100 mV	15.7%	6494	14.9%
	150 mV	15.1%	6522	14.3%
	200 mV	17.2%	6543	16.2%
	250 mV	8.5%	6337	15.2%
	300 mV	6.0%	6297	13.4%
O ₂	100 mV	13.9%	6178	15.3%
	150 mV	14.2%	6154	13.9%
	200 mV	15.2%	6231	15.5%
	250 mV	7.8%	6177	15.4%
	300 mV	5.3%	6219	14.6%
Ar	100 mV	17.5%	6229	20.6%
	150 mV	17.4%	6257	19.9%
	200 mV	18.5%	6158	19.9%
	250 mV	12.3%	6125	17.7%
	300 mV	6.8%	6087	18.4%

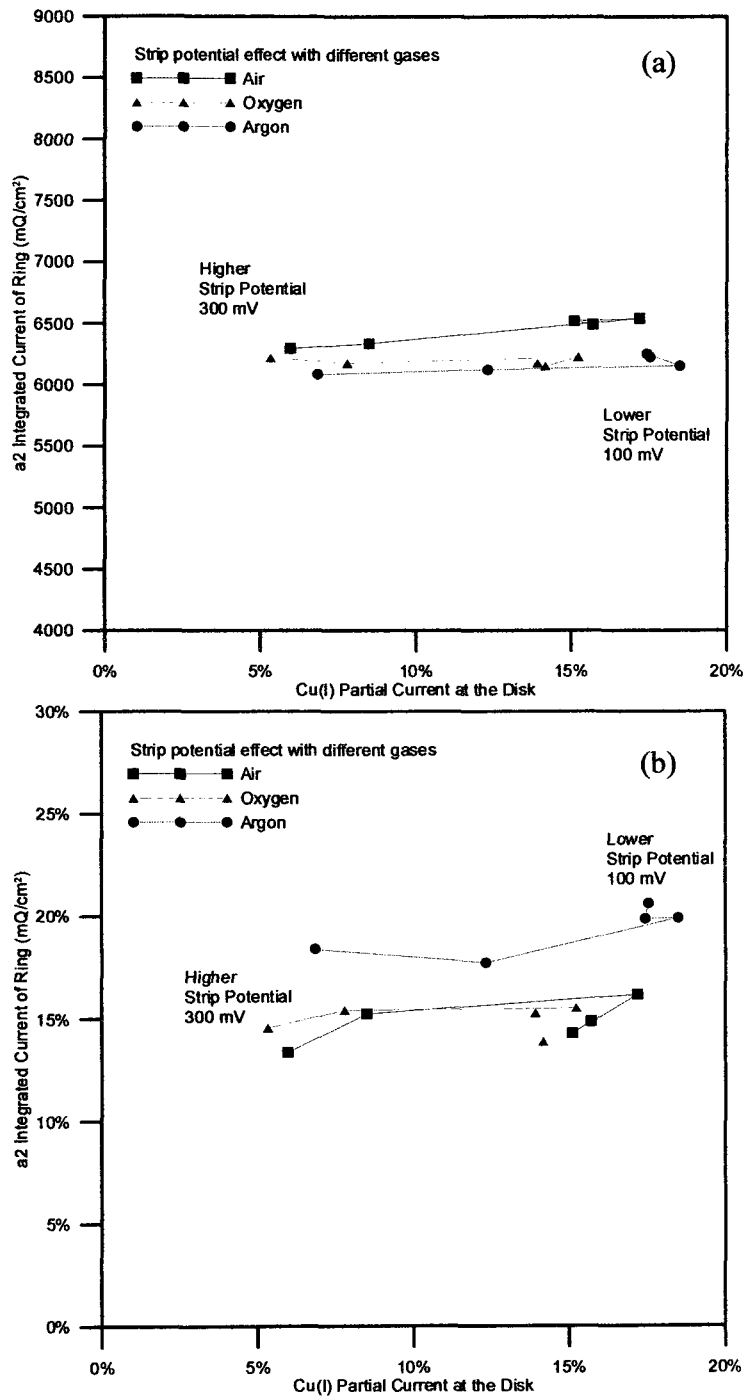


Figure 4.21 (a) Average ring charge with Cu (I) generation, and (b) Increased percentage of ring charge from a1 to a2 as a function of Cu (I) partial current at disk by strip potential variation under air, oxygen, and argon.

CHAPTER V: CONCLUSIONS AND RECOMMENDATIONS FOR FUTURE WORK

5.1 Conclusions

The focus of this work is the hypothesis that the accelerant in the PEG/Cl⁻/SPS additive system is produced by a reaction of SPS or a derivative of SPS with Cu (I). If this link can be established quantitatively, it could lead to design of new processes for filling of through-silicon vias or other commercially important structures in semi-conductor packaging. To validate and quantify this mechanism, interactions among SPS, Cu (I), and oxygen were studied on rotating ring-disk electrode. The independent variables were SPS concentration, strength of forced convection, production of Cu (I) at the disk electrode and the concentration of dissolved oxygen. The dependent variable was the rate of deposition on the ring.

When SPS is present in the solution, a sudden kinetic acceleration is observed at the ring during Cu (I) generation at the disk. By comparison of the ring deposition rate without and with Cu (I) generation at the disk, it is found that the deposition current increases with SPS concentrations from 4 to 10 ppm, and then saturates with SPS concentrations up to 40 ppm. This result is consistent with the hypothesis that the true accelerant is formed by homogeneous reaction of SPS and Cu (I). Furthermore, it suggests that the limiting reactant in generation of accelerant is Cu (I).

When the rotation speed is increased, enhanced convective-diffusion affects both the ratio of Cu (I) generation at the disk and the acceleration at the ring. The accelerant is not produced without effective transport of Cu (I) from the disk. This is supported by the

small increases in ring current observed at low rotation speeds of 5 to 10 rpm. At the higher rotation speed from 25 to 400 rpm a much greater increases in ring charge is observed.

To establish the central role of Cu (I), the effect of acceleration at the ring was correlated with the partial current of Cu (I) generation at the disk. Each of the independent variables, additive concentration, rotation speed, purge, gas, has an effect on the Cu (I) partial current. In the presence of additives, the ratio of Cu (I) partial current at the disk to total stripping current at the disk is highly dependent on rotation speed. The Cu (I) ratio is about 4% lower under oxygen while it is about 2% higher under argon compared to the condition under air. For the solution without additives, Cu (I) generation at the disk is 10 times smaller than in solution with additives. In relation to SPS concentration, purge gas and rotation speed, the calculated Cu (I) partial currents are good predictors of the accelerant effect at the ring, as we would expect from our hypothesis. However, the disk stripping potential, which generates a wide variation in Cu (I) partial current has little effect on acceleration at the ring. This result is difficult to understand solely in terms of the hypothesis that Cu (I) is the limiting reactant in generation of accelerant. Hence, additional study on this issue would be valuable.

5.2 Recommendations for future work

The following recommendations are suggested to further study the interactions among SPS, Cu (I), and oxygen.

1. The gas flow rate and duration of gas purging may be other factors to affect the interactions. It may be desirable to devise a method for direct measurement of the

dissolved oxygen concentration.

2. The location inside the vessel where oxygen or argon is directly purged also affects the results. If the purging tube is placed at the bottom of reaction vessel, its influence is the most obvious. However, unpredictable gas-induced turbulence causes non-reproducible results.
3. The disk-stripping potential influences Cu (I) generation at the disk. However, it does not influence acceleration at the ring, which appears to contradict other results. The Cu (I) partial current was calculated based on a mol balance on the deposition and stripping charges. It would be valuable to look more closely into the Cu (I) partial current and find a more rigorous theoretical or experimental means to determine it.

LITERATURE CITED

1. P. C. Andricacos, C. Uzoh and J. O. Dukovic, Damascene copper electroplating for chip interconnections, *IBM Journal of Research and Development*, **42**, 567 (1998).
2. J. Lipkowski and P. N. Ross, *Adsorption of molecules at metal electrodes*, p. xi, VCH, New York, NY (1992).
3. W. Plieth, Additives in the electrocrystallization process, *Electrochim Acta*, **37**, 2115 (1992).
4. L. Oniciu and L. Muresan, Some fundamental aspects of levelling and brightening in metal electrodeposition, *Journal of Applied Electrochemistry*, **21**, 565 (1991).
5. T. C. Franklin, Some mechanisms of the action of additives in electrodeposition processes, *Plat Surf Finish*, **81**, 62 (1994).
6. S. Trasatti, Adsorption of organic-substances at electrodes - recent advances, *Electrochim Acta*, **37**, 2137 (1992).
7. A. J. Bard and L. R. Faulkner, *Electrochemical methods : Fundamentals and applications*, p. xxi, Wiley, New York (2001).
8. D. M. Soares, S. Wasle, K. G. Weil and K. Doblhofer, Copper ion reduction catalyzed by chloride ions, *J Electroanal Chem*, **532**, 353 (2002).
9. S. Yoon, M. Schwartz and K. Nobe, Rotating-ring-disk electrode studies of copper electrodeposition - effect of chloride-ions and organic additives, *Plat Surf Finish*, **81**, 65 (1994).
10. W. Shao, G. Pattanaik and G. Zangari, Influence of chloride anions on the mechanism of copper electrodeposition from acidic sulfate electrolytes, *Journal of the Electrochemical Society*, **154**, D201 (2007).
11. D. Stoychev and C. Tsvetanov, Behaviour of poly(ethylene glycol) during electrodeposition of bright copper coatings in sulfuric acid electrolytes, *Journal of Applied Electrochemistry*, **26**, 741 (1996).
12. J. J. Kelly and A. C. West, Copper deposition in the presence of polyethylene glycol - i. Quartz crystal microbalance study, *Journal of the Electrochemical Society*, **145**, 3472 (1998).
13. J. J. Kelly and A. C. West, Copper deposition in the presence of polyethylene glycol - ii. Electrochemical impedance spectroscopy, *Journal of the Electrochemical Society*, **145**, 3477 (1998).
14. J. P. Healy, D. Pletcher and M. Goodenough, The chemistry of the additives in an acid copper electroplating bath .1. Polyethylene-glycol and chloride-ion, *J Electroanal*

Chem, **338**, 155 (1992).

15. J. P. Healy, D. Pletcher and M. Goodenough, The chemistry of the additives in an acid copper electroplating bath - the instability of 4,5-dithiaoctane-1,8-disulfonic acid in the bath on open circuit, *J Electroanal Chem*, **338**, 167 (1992).

16. D. S. Stoychev, I. Vitanova, S. Rashkov and T. Vitanov, Adsorption of substances acting as brighteners in the electrolytic deposition of copper, *Surface Technology* **7**(1978).

17. G. A. Hope, G. M. Brown and D. P. Schweinsberg, Observations of inclusions of polymeric additives in copper electrodeposits by transmission electron microscopy, *Journal of Applied Electrochemistry*, **25**, 890 (1995).

18. S. A. U. Ibrahim, *Study of additives used in a copper via filling chemistry*, in *Chemical Engineering*, p. 112, University of New Hampshire, Durham, NH (2009).

19. W.-P. Dow, M.-Y. Yeng and W.-B. Lin, Influence of molecular weight of polyethylene glycol on microvia filling by copper electroplating, *Journal of the Electrochemical Society*, **152**, C769 (2005).

20. W.-P. Dow and H.-S. Huang, Roles of chloride ion in microvia filling by copper electrodeposition. I. Studies using sem and optical microscope, *Journal of the Electrochemical Society*, **152**, C67 (2005).

21. K. R. Hebert, Role of chloride ions in suppression of copper electrodeposition by polyethylene glycol, *Journal of the Electrochemical Society*, **152**, C283 (2005).

22. C. C. Hung, W. H. Lee, S. C. Chang, K. W. Chen and Y. L. Wang, Suppression effect of low-concentration bis-(3-sodiumsulfopropyl disulfide) on copper electroplating, *Journal of the Electrochemical Society*, **155**, D133 (2008).

23. K. Kondo, T. Yonezawa, D. Mikami, T. Okubo, Y. Taguchi, K. Takahashi and D. P. Barkey, High-aspect-ratio copper-via-filling for three-dimensional chip stacking - ii. Reduced electrodeposition process time, *Journal of the Electrochemical Society*, **152**, H173 (2005).

24. T. Okubo, K. Watanabe and K. Kondo, Analytical study of the characteristics of cu(i) species for the via-filling electroplating using a rrde, *Journal of the Electrochemical Society*, **154**, C181 (2007).

25. P. M. Vereecken, R. A. Binstead, H. Deligianni and P. C. Andricacos, The chemistry of additives in damascene copper plating, *IBM Journal of Research and Development*, **49**, 3 (2005).

26. T. P. Moffat, D. Wheeler and D. Josell, Electrodeposition of copper in the sps-peg-cl additive system - i. Kinetic measurements: Influence of sps, *Journal of the Electrochemical Society*, **151**, C262 (2004).

27. M. Tan, C. Guymon, D. R. Wheeler and J. N. Harb, The role of sps, mpsa, and chloride in additive systems for copper electrodeposition, *Journal of the Electrochemical Society*, **154**, D78 (2007).
28. D. Josell, D. Wheeler, W. H. Huber, J. E. Bonevich and T. P. Moffat, A simple equation for predicting superconformal electrodeposition in submicrometer trenches, *Journal of the Electrochemical Society*, **148**, C767 (2001).
29. R. Akolkar and U. Landau, A time-dependent transport-kinetics model for additive interactions in copper interconnect metallization, *Journal of the Electrochemical Society*, **151**, C702 (2004).
30. R. Akolkar and U. Landau, Mechanistic analysis of the "Bottom-up" Fill in copper interconnect metallization, *Journal of the Electrochemical Society*, **156**, D351 (2009).
31. D. P. Barkey, K. Kondo, T. Matsumoto and A. Wu, in *AIChE Annual Meeting*, p. 189f (2003).